Marine and Petroleum Geology 124 (2021) 104822

Contents lists available at ScienceDirect

Marine and Petroleum Geology

journal homepage: www.elsevier.com/locate/marpetgeo

Research paper

Forward numerical modelling constraining environmental parameters (Aptian carbonate system, E Iberia)

Òscar Gratacós [a,d,*], Telm Bover-Arnal [b,d], Roger Clavera-Gispert [c], Ana Carmona [e], David García-Sellés [a,d]

[a] Departament de Dinàmica de la Terra i de l'Oceà, Facultat de Ciències de la Terra, University of Barcelona, Martí i Franquès, s/n, Barcelona, 08028, Spain
[b] Departament de Mineralogia, Petrologia i Geologia Aplicada, Facultat de Ciències de la Terra, Universitat de Barcelona, Martí i Franquès s/n, 08028, Barcelona, Spain
[c] GEOMAR Helmholtz-Zentrum für Ozeanforschung Kiel, Marine Geodynamik, Wischhofstrasse 1-3, 24148, Kiel, Germany
[d] Institut de Recerca Geomodels, Facultat de Ciències de la Terra, Universitat de Barcelona, Martí i Franquès, s/n, Barcelona, 08028, Spain
[e] External Consultant, Institut de Recerca Geomodels, Facultat de Ciències de la Terra, Universitat de Barcelona, Martí i Franquès, s/n, Barcelona, 08028, Spain

ARTICLE INFO

Keywords:
Carbonate production
Sea-level change
Environmental parameters
Forward modelling
Process-based modelling

ABSTRACT

The facies distribution in time and space of sedimentary successions is controlled by a complex interplay between physical, chemical and biological processes, which are nowadays difficult to construe from the geological record. Numerical models constitute a valuable tool to identify and quantify such controlling factors permitting a reliable 3D extrapolation and prediction of stratigraphic and facies architectures beyond outcropping rock strata. This study assesses the roles of three controlling parameters being carbonate production rate, relative sea-level changes and terrigenous clastic sediment supply, on the evolution of an Aptian carbonate system. The SIMSAFADIM-CLASTIC, a 3D process-based sedimentary-stratigraphic forward model, was used for this evaluation. The carbonate succession modelled crops out in the western Maestrat Basin (E Iberia), and corresponded to a platform-to-basin transition comprising three depositional environment-related facies assemblages: platform top, slope and basin. Testing of geological parameters in forward modelling results in a wide range of possible 3D geological scenarios. The documented distribution of facies and sequence-stratigraphic framework combined with a virtual outcrop model were used as a reference to perform geometric (quantitative) and architectural and stacking pattern (qualitative) research by model-data comparison. The time interval modelled spans 1450 ky. The best-fit simulation run characterizes and quantifies (1) relative sea-level fluctuations recording five different genetic types of deposit (systems tracts) belonging to two depositional sequences as expected from field-data analysis, (2) a rate of terrigenous clastic sediment input ranging between 0.5 and 2.5 gr/s, and (3) a mean autochthonous carbonate production maximum rate of 0.08 m/ky. Furthermore, the quantitative and qualitative sensitivity tests carried out highlight that the fluctuation of relative sea level exerted the main control on the resulting stratigraphic and facies architectures, whereas the effect of inflowing terrigenous clastic sediment is less pronounced. Facies assemblages show different sensitivities to each parameter, being the slope carbonates more sensitive than the platform top facies to inflowing fine terrigenous sediments. On slope depositional settings, siliciclastic input also controls stratal stacking patterns and the dimensions of the carbonate bodies formed. The final 3D model allows to spot architectural features such as stacking patterns that can be misinterpreted by looking at the resulting record in the outcrop or by using other 2D approaches, and facilitates the comprehension of reservoir connectivity highlighting the occurrence of initial disconnected regressive platforms, which were later connected during a transgressive stage.

* Corresponding author. Departament de Dinàmica de la Terra i de l'ceà Facultat de Ciències de la Terra, University of Barcelona, Martí i Franquès, s/n, 08028, Barcelona, Spain.
E-mail addresses: ogratacos@ub.edu (Ò. Gratacós), telm.boverarnal@ub.edu (T. Bover-Arnal), rclavera-gispert@geomar.de (R. Clavera-Gispert), anacarmonabardella@gmail.com (A. Carmona), dgarcia@ub.edu (D. García-Sellés).

https://doi.org/10.1016/j.marpetgeo.2020.104822
Received 30 June 2020; Received in revised form 4 November 2020; Accepted 16 November 2020
Available online 20 November 2020

1. Introduction

Understanding the dynamics of sedimentary basins is an essential point in geological research to better predict the 3D distribution and geometry of sedimentary bodies relevant to exploration and exploitation of natural resources. The physical, chemical and biological processes that control these dynamic systems, as well as their controlling parameters and complex relationships, are thus main factors that need to be considered.

However, our ability to observe the geology in 3D and/or to extract all relevant information from the geological record is limited. Not only due to the number and quality of the outcrops, but also to the fact that the parameters and relationships that controlled past geological processes are hidden in the sedimentary record. Subsurface or indirect geological data can provide valuable information of sedimentary basins under exploration. Nevertheless, these datasets are commonly limited to seismic-scale architectural frameworks (e.g., Abreu, 1998; Posamentier and Kolla, 2003) and borehole-based petrophysical properties of discrete sedimentary successions (e.g., Plint, 1988; Borgomano et al., 2008).

Numerical modelling, and specifically Stratigraphic Forward Models (SFM), represents a valuable complement to fill the information gaps, allowing a better understanding of the behaviour of the studied system when it experienced different environmental conditions, and thus, permits to generate spatial and temporal predictions of facies distributions (Griffiths, 1996; Syvitski and Hutton, 2001). In this regard, modelling permits to constraint the values of the controlling parameters of the geological processes considered (e.g., initial bathymetry, relative sea-level oscillation, carbonate sediment production) and setting the relationship between them. The interplay between the controlling parameters considered and their tested ranges also give rise to possible scenarios of sediment distribution using SFM. These scenarios can be used for a model-data comparison in order to find the best-fit scenarios, thus a) constraining the range value of the controlling parameters, and b) increasing the prediction capacity through the selected model. Furthermore, not only the best-fit approximation model obtained from numerical modelling is of relevance, but also the discarded scenarios may constitute knowledge or provide key information to understand the evolution of other basins with analogue characteristics in a more efficient way.

In this paper, we apply a 3D stratigraphic process-based forward numerical model (the SIMSAFADIM-CLASTIC code, SF-CL, developed at the Geomodels Research Institute at the University of Barcelona) to an Aptian carbonate system from the Maestrat Basin (E Iberia). The SF-CL is a 3D process-based numerical forward model, which simulates processes of autochthonous marine carbonate production and accumulation through modelling carbonate producing organisms' evolution and interactions between species associations. These processes are coupled with processes of subaqueous clastic transport and sedimentation in three dimensions of both carbonate and terrigenous sediments. The main parameters and processes modelled by SF-CL are summarized in Fig. 1. Initially developed by Bitzer and Salas (2002), Gratacós (2004), and Gratacós et al. (2009a, 2009b) was later modified and improved by Clavera-Gispert (2016) and Clavera-Gispert et al. (2012, 2017). These improvements include the Generalized Lotka-Volterra equation to model the evolution of unlimited number of carbonate producing species associations, and introduce their evolution as a function of: (1) the environment (slope, energy, light and sediment in suspension), (2) intrinsic factors of each species association; and (3) interactions among all the modelled species association (Clavera-Gispert et al., 2012). The SF-CL program has also been used to model syntectonic sedimentation allowing the simulation of sedimentary processes (provided by the SF-CL program) together with tectonic deformation processes through a kinematic and mechanic discrete element model (DEM) (e.g., Finch et al., 2003; 2004; Hardy and Finch, 2005). From this linkage, much more complex and realistic depositional structures can be simulated with the new code (Carmona, 2016; Carmona et al., 2010, 2016) as tectonic processes control sedimentary deposits, which, in turn, also exerts control over tectonic processes.

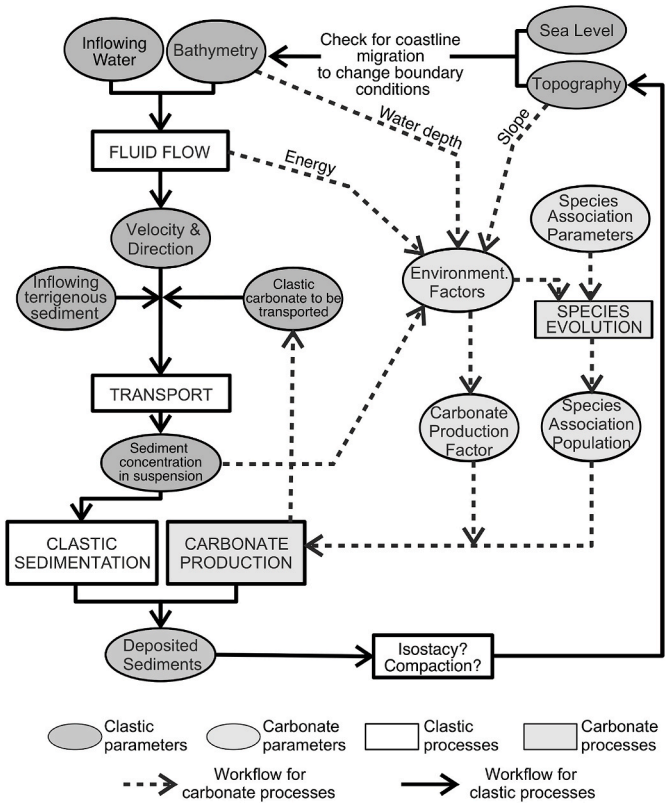

Fig. 1. Main processes and parameters and their relationships modelled by the SIMSAFADIM-CLASTIC program.

The aim of this work is to use a forward-numerical process-model (SF-CL) to (1) determine and quantify the main factors that controlled carbonate production and accumulation in an Aptian carbonate system from the Maestrat Basin, (2) to establish the relationship among the controlling variables, and (3) to model the distribution in time and space of the different carbonate facies and stratal stacking patterns. The growth of the carbonate system modelled occurred along a platform-to-basin transition (Bover-Arnal et al., 2009, 2010), and was governed by the interplay of several controlling parameters including relative sea level (RSL), carbonate production, and input of terrigenous sediments. The different value ranges tested for these controlling parameters and their combination results in a wide range of possible 3D geological scenarios that are summarized and discussed. Thus, the resulting simulations and quantifications of the environmental parameters obtained could be of relevance to better constrain the growth, architecture and facies heterogeneities of coeval carbonate platforms from other basins worldwide including giant subsurface hydrocarbon reservoirs such as the Shu'aiba Formation in the Middle East.

2. Geological overview

The platform-to-basin transition area modelled has been widely studied in terms of sequence stratigraphy and sedimentology (Bover-Arnal et al., 2009, 2010, 2011, 2012; Bover-Arnal and Salas, 2010) (Figs. 2–4). The field data and the sequence-stratigraphic framework simulated in this paper are taken from these latter publications. However, alternative interpretations to the sequence-stratigraphic analysis carried out by Bover-Arnal et al. (2009) exist (Peropadre et al., 2013; Pomar and Haq, 2016; Pomar, 2020). Next, a brief geological setting is provided.

2.1. Study area

The Maestrat Basin is one of the Iberian intraplate rift basins that developed as a result of the spreading of the Atlantic Ocean and the opening of the Bay of Biscay throughout late Oxfordian to early late Albian times. Later, during the Paleogene, the Alpine orogeny caused the inversion of the Iberian Mesozoic rifts and gave rise to the Iberian Chain in the northeastern Iberian Peninsula (Salas and Casas, 1993; Salas et al., 2001; Salas et al. in Martín-Chivelet et al., 2019). The platform margin reconstructed here is of late early Aptian age, it has an extension of 1.2 km^2 and is situated in the central Galve sub-basin, which conforms the western marginal part of the Maestrat Basin (E Iberian Chain) (Fig. 2). The carbonate succession tackled is located in Las Mingachas, to the west of the village of Miravete de la Sierra in the province of Teruel (E Spain) (Fig. 2). It crops out in the western limb of an anticline structure slightly tilted towards the southwest around 9° (Vergés et al., 2020). The age of these rocks was determined by means of strontium-isotope stratigraphy, as well as ammonite, orbitolinid and rudist biostratigraphies (Bover-Arnal et al., 2009, 2010, 2016; Moreno-Bedmar et al., 2010). The strata modelled comprise the marls of the upper part of the Forcall Formation, the platform carbonates of the Villarroya de los Pinares Formation and the marls and limestones of the lower part of the Benassal Formation (Canérot et al., 1982; Vennin and Aurell, 2001; Bover-Arnal et al., 2009, 2010, 2016; Embry et al., 2010) (Fig. 3). The sedimentary succession is distinguished by lithofacies heterogeneity and superb clinobeds and stratal terminations (Fig. 4), which permit to construe three different depositional settings: platform top, slope and basin (Bover-Arnal et al., 2009).

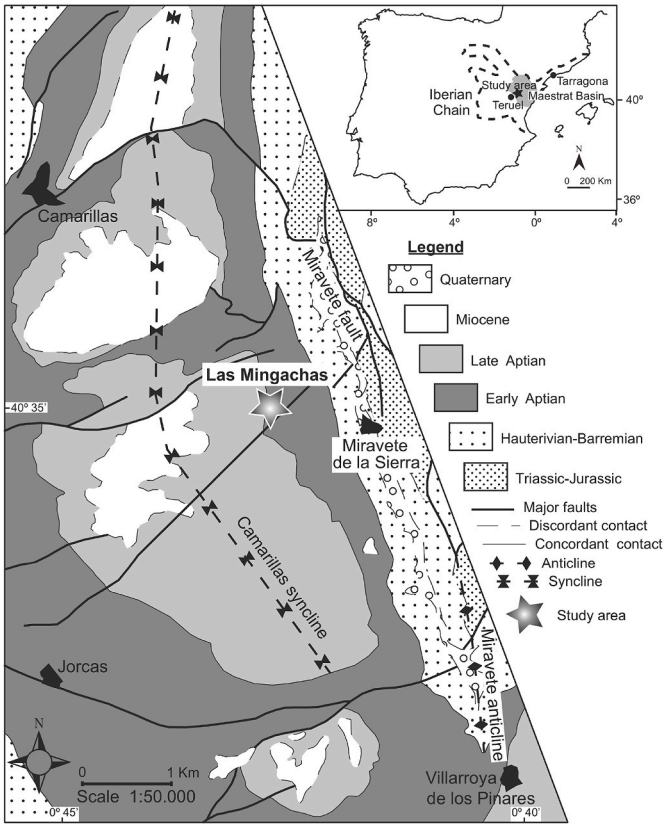

Fig. 2. Geological map of the study site with its position inside Iberia. The situation of Las Mingachas platform-to-basin transition area modelled is indicated with a star. Modified from Bover-Arnal et al. (2009).

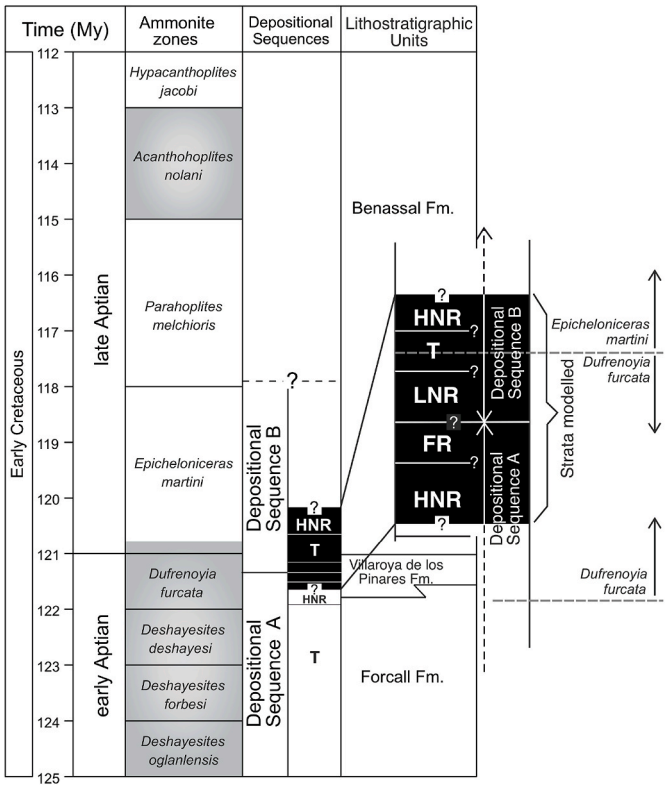

Fig. 3. Synthetic overview of the lithostratigraphy and age relationships of the Aptian in the central Galve sub-basin. The strata modelled are indicated by a black rectangle and detailed in the enlarged image (see Figs. 2 and 4 for the location of the modelled strata). The ammonoid biozones recognized are marked in grey. Absolute ages are taken from Gradstein et al. (2004). Key (see also Fig. 3): T = Transgressive, HNR=Highstand Normal Regressive, FR=Forced Regressive, LNR = Lowstand Normal Regressive. Modified from Bover-Arnal et al. (2009).

2.2. Facies assemblages

In order to pursue the numerical modelling of stratal architecture and sedimentary heterogeneities, three different facies associations (platform top, slope and basin marls) were determined along the platform-to-basin profile anatomized. To facilitate the model setup and validation, the facies assemblages characterized differ from the ones established by Bover-Arnal et al. (2009, 2010) in that are representative of main depositional settings, and thus were not distinguished on the basis of lithology, rock textures and petrographic components.

2.2.1. Facies assemblage I (FA I): platform top

This facies assemblage is characterized by decimetre- to meter-scale light grey beds of *in situ* platform top carbonates (Fig. 5A) with floatstone and rudstone fabrics and biostromes dominated by rudist bivalves and corals in life position. Polyconitid rudists are grouped in clusters (Fig. 5B). Corals exhibit abundant *Lithophaga* borings and are present in five different morphologies: sheet-like, platy, branching, irregular massive and domal. Orbitolinids, miliolids, other benthic foraminifera, *Chondrodonta*, oysters, unidentified bivalves, nerineid gastropods, bryozoans, echinoderms, calcareous algae, peloids and encrusting *Lithocodium aggregatum* and sessile foraminifera, are also common. The beds are massive, tabular, or occasionally show nodular bedding. Local bioturbated levels occur.

2.2.2. Facies assemblage II (FA II): slope

Resedimented carbonates shed from platform top (Lithofacies Assemblage I) accumulated along slope environments (Fig. 5A). On

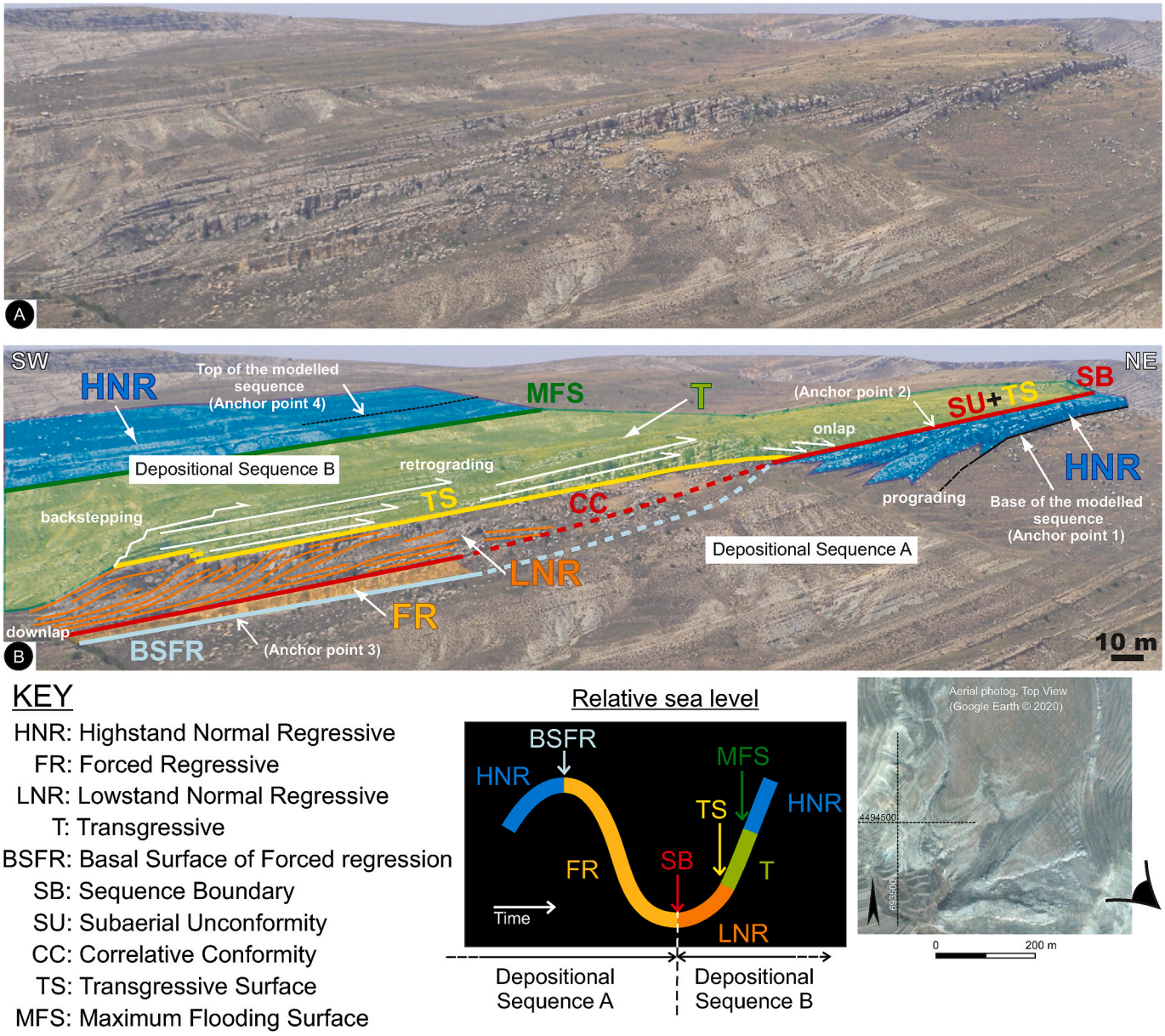

Fig. 4. A) Panoramic view of the platform-to-basin transition at Las Mingachas. B) Sequence-stratigraphic interpretation of image A with the five different stages of relative sea-level recognized (see coloured legend). The base and the top of the modelled stratigraphic interval it is also marked (anchor points 1 to 4, see text). Modified from Bover-Arnal et al. (2009). An aerial top view of the studied area with the oblique view localisation can be shown at the lower right image.

occasions, the beds occur in the form of channels and/or exhibit erosive surfaces such as slump scars. This facies association is marked by light grey, nodular limestones exhibiting very poorly sorted floatstone to rudstone textures, which contain fragmented skeletal components of the biotic communities detailed in Facies Assemblage I (Fig. 5C). The skeletal components of these redeposited carbonates show angular edges and are commonly encrusted by *Lithocodium aggregatum*, peyssonneliaceans and sessile foraminifera. The beds display decimetre- to meter-scale thicknesses and exhibit a chaotic organization. The dip angles measured on the lowstand slopes range between 5 and 25° (Fig. 5A).

The slope deposits are also characterized by the presence of centimetre- to meter-scale marly intervals intercalated between the carbonates shed from platform top (Fig. 5A). The marly slope facies contain isolated coral colonies (Fig. 5D) and small patch-reefs, polyconitid rudists grouped in clusters and *Chondrodonta*, among other molluscs, echinoids and ammonoids. The corals have widths ranging between centimetres and meters, show abundant *Lithophaga* borings and occur in growth position exhibiting domal (Fig. 5D), branching and irregular massive forms.

2.2.3. *Facies assemblage III (FA III): basin marls*

The facies assemblage consists of centimetre- to meter-scale alternations of marls and mudstone to floatstone yellowish and greyish limestones (Fig. 5E) displaying massive or nodular bedding. The limestones often present silt-sized quartz grains. The occurrence of calcareous nodules in the marls and interbedded centimetre- to decimetre-scale beds of nodular limestones and fine-grained graded sandy/silty limestones with plane-parallel stratification interpreted as turbidites are also characteristic. *Thalassinoides* on bed bases and highly bioturbated levels with unidentified burrows occur. The basin facies association is distinguished by the presence of orbitolinids (Fig. 5F), ammonites, nautiloids, gastropods, bryozoans, echinoderms, solitary corals, brachiopods, sessile foraminifera, oysters, unidentified bivalves, decapods, hydrozoans, fish teeth and pyritized skeletal components. The size of the

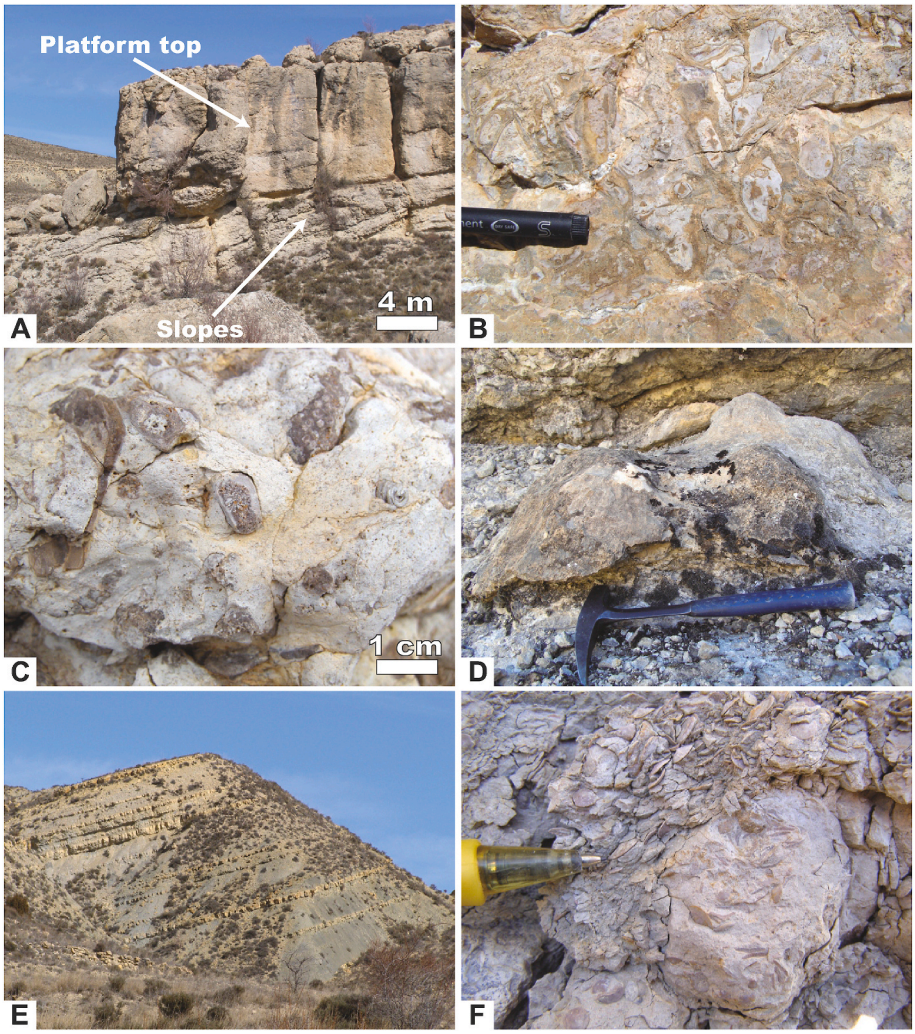

Fig. 5. Outcrop photographs and photomicrographs of the three different facies assemblages determined. A) Outcrop photograph of a platform-to-slope transition. Note the massive aspect of the *in situ* platform top facies (Facies Assemblage I) and the nodular bedding of the slope resedimented carbonate deposits (Facies Assemblage II). B) Detail of the platform top facies (Facies Assemblage I). Note the polyconitid rudists in growth position grouped in a cluster. Pen = 4.5 cm. C) Close-up view of resedimented slope deposits (Facies Assemblage II). Note the presence of skeletal fragments of corals, rudist bivalves and gastropods. D) Detail of an isolated coral colony belonging to the marly slope environments (Facies Assemblage II). Note the domal morphology exhibited by the colony. Hammer = 32 cm. E) Outcrop view of the basin marls of the Forcall Formation (Facies Assemblage III). Width of image is *c*. 50 m. F) Close-up view of basin marls containing abundant orbitolinids (Facies Assemblage III). Pen = 2 cm.

skeletal components ranges from 1 mm to few cm, to dm in the case of ammonoids and nautiloids.

2.3. Sequence-stratigraphic analysis

The sequence-stratigraphic analysis performed by Bover-Arnal et al. (2009, 2011) and Bover-Arnal and Salas (2010) in the platform-to-basin transition domain of Las Mingachas is in agreement with the four systems tract-based sequence-stratigraphic method of Hunt and Tucker (1992, 1995). For the present paper, however, the sequence stratigraphic nomenclature was modified and brought up-to-date applying the standardized terminology proposed by Catuneanu et al. (2009).

Five different genetic types of deposit (systems tracts) belonging to two distinct depositional sequences, A and B, can be interpreted from the sedimentary record of Las Mingachas (Fig. 4). The upper part of Depositional Sequence A is composed of a Highstand Normal Regressive (HNR) lithostratigraphic unit followed by Forced Regressive (FR) deposits. These normal and forced regressive strata are of late early Aptian age. Depositional Sequence B comprises a Lowstand Normal Regressive (LNR) genetic unit followed by Transgressive (T) deposits and the subsequent return to a highstand stage of relative sea level (HNR). Depositional Sequence B spans the uppermost latest early-earliest late Aptian time interval.

The HNR of Depositional Sequence A corresponds to a large and extensive flat-topped non-rimmed carbonate platform, which exhibits a high rate of carbonate production stacked in an aggrading-prograding pattern, and downlapping stratal terminations (Fig. 4). This highstand genetic type of deposit is made up of platform top facies (FA I; Fig. 5A–B), which change basinwards to slope facies (FA II; Fig. 5A and 5C-D) and then, to basin marls (FA III; Fig. 5E–F). The outcropping sections of the highstand slopes are oblique views (Fig. 4), thus the real dip angles of the highstand slopes cannot be measured in the ouctrop.

During base-level fall, a detached cross-bedded calcarenitic wedge constituted by packstone and grainstone textures with benthic foraminifera, intraclasts and fragments of calcareous algae, corals, echinoids and molluscs accumulated at the toe of the former highstand slope, in a basinal position. This hydrodynamically-influenced basin floor component with reworked shallow-water components overlies deeper-water highstand basinal marls, and is thus interpreted as a forced regression. The FR unit is bounded below by the Basal Surface of Forced Regression (BSFR) and above by the Sequence Boundary (SB), which delimits depositional sequences A and B (Fig. 4). The BSFR marks the start of RSL fall at the shoreline, while the SB was formed at the lowest point of RSL. During this FR stage, the HNR carbonate platform was exposed subaerially and partially eroded, therefore a Subaerial Unconformity (SU), which passes basinwards to its marine Correlative Conformity (CC), surmounts the highstand platform (Fig. 4).

Above the CC, the LNR genetic unit of Depositional Sequence B comprises the sediments deposited during the stillstand and the subsequent base-level rise. These deposits correspond to a small flat-topped non-rimmed carbonate platform stacked in a prograding-aggrading pattern, which onlaps landwards and downlaps over the FR unit and

thus, onto the CC (Fig. 4). Similar to the HNR unit of Depositional Sequence A, the LNR is constituted by platform top facies (FA I; Fig. 5A–B), which change laterally to slope facies (FA II; Fig. 5A, C-D).

The Transgressive Surface (TS) marks the start of transgression at the shoreline and establishes the boundary between the lowstand platform and the Transgressive (T) genetic type of deposit. Above this surface, the small prograding lowstand platform starts to backstep evolving to marly deposits upwards in the succession, after local drowning (Fig. 4). Landwards, the TS is superposed onto the SU, resulting in a composite surface. The T deposits correspond to platform top facies (Facies Assemblage I; Fig. 5A–B), which pass upwards in the succession and basinwards to distal slope and basin marls (FA III; Fig. 5E–F).

The Maximum Flooding Surface (MFS) separates the T unit (below) from the subsequent HNR (above). This surface was placed at the top of the thickest T marly interval owing to the absence of fauna or a surface with physical characteristics that may be indicative of the maximum bathymetry reach during Depositional Sequence B. Above the MFS, the establishment of new carbonate platforms characterizes a new highstand stage of RSL (Fig. 4). The carbonate deposits of the HNR of Depositional Sequence B display a ramp-like depositional profile and are thinner than those previously described for the HNR of Depositional Sequence A (Fig. 4). These deposits belonging to the lower part of the Benassal Formation are actually eroded towards the northeast.

On the other hand, in Las Mingachas, Peropadre et al. (2013) recognized a transgressive systems tract followed by two regressive systems tracts, and four regional composite scour surfaces. The basin floor wedge interpreted by Bover-Arnal et al. (2009) as a forced regression was regarded by Peropadre et al. (2013) as the uppermost part of a transgressive systems tract. Pomar and Haq (2016) acted as arbiters between the two interpretations and endorsed the view of Peropadre et al. (2013). More recently, the interpretation of this sedimentary unit as a regression by Bover-Arnal et al. (2009) has been again discredited by Pomar (2020).

3. Modelling approach

3.1. Methods

Numerical models were constructed using the SF-CL code. This program is coded in Fortran 95 programming language and uses a finite element (FE) method to discretize the studied basin and to solve the main equations describing the main geological processes modelled. The main parameters and processes modelled by SF-CL are summarized in Fig. 1. Defining the inflowing (water discharge in m^3/s) and outflowing (fixed potential in m) areas, a 2D potential flow is established. Thus, the fluid-flow system is modelled through a 2D potential flow model taking into account a variable flow in function of the water depth (Bitzer and Salas, 2002). The code uses the advective-diffusive-dispersive terms to simulate clastic transport processes. When the system is advective-dominated, transport of clastic particles in suspension can be calculated in function of the flow velocity that, in turn, is used to calculate sedimentation. In function of the flow velocity, the settling velocity can be obtained for each particle size. Then, from a threshold velocity below which sedimentation takes place (defined by the user for each clastic sediment type), the maximum settling velocity (also defined by the user for each sediment type) decreases in function of the flow velocity in each node of the FE mesh, being 0 when only transport occurs just above the threshold velocity. When the flow velocity is 0, transport happens through a diffusive term (for a more detailed explanation see Gratacós, 2004 and Gratacós et al., 2009a). In its current program version, no erosional or diagenetic processes are modelled.

Autochthonous marine carbonate production and accumulation can also be modelled by the program through an ecological model (Clavera-Gispert et al., 2012, 2017). The program models the evolution of the organism's associations (and their interactions) in function of environmental factors such as water depth (light), slope, energy (fluid flow), nutrients and sediment in suspension. These factors and their influences are set by the user between 0 and 1 using trapezoidal functions (Clavera-Gispert et al., 2017) that control the population of the associations and the final volume of carbonate produced for each species association. To consider the total amount of carbonate accumulated, lime and clastic carbonate sediment types are also modelled. The user can define the maximum carbonate lime produced that is in function of the carbonate producing organisms' population and their environmental factors. The user can also set the proportion of this carbonate lime produced that can be settled *in situ* or can be transported in suspension as the other clastic sediments. As no erosional processes are considered, in order to simulate resedimented clastic carbonate sediments due to erosion, the user can set a clastic carbonate production that can be transported and sedimented as clastic sediment in function of the fluid-flow system. The program also includes variables such as sea-level changes, subsidence, isostacy and compaction.

SF-CL output is stored in a 3D volume defined by cells in which the horizontal dimension is set by the FE mesh and the vertical dimension is calculated from the total amount of sediment deposited in each time step. Different properties can be displayed: the total amount of sediment deposited (in m), the sediment percentage and the sediment deposited (in m) for each sediment type. Sediment percentage is finally used to obtain the facies assemblages represented by a colour coded in function of the dominant sediments. A 2D-mesh located at the relative sea-level (RSL) elevation for every time-step it can be also displayed. This 2D mesh shows the sediment concentration that rests in suspension for each clastic sediment type, the distribution of carbonate-producing species associations, the fluid-flow system (magnitude and direction), the boundary conditions (open-closed boundaries and inflowing nodes), the coastline location, and the environmental factors applied for each carbonate-producing assemblage. Input parameters are set through ASCII input files that can be defined in each time step in order to introduce changes in the input parameters along the modelled time. Output results are stored in ASCII output files (".txt" and ".vtk" format) that can be displayed with an open-source multi-platform data analysis and visualization application such as Paraview (http://www.paraview.org/).

3.2. Workflow and constraints

The previous sequence-stratigraphic analysis interpreted at Las Mingachas and the three facies associations described have been used as a reference platform to perform the stratigraphic forward models by means of SF-CL software from an architectural and stratal stacking patterns (qualitative), as well as geometric (quantitative) point of views. The workflow followed is summarized in Fig. 6.

As explained in the previous section, the available geological data from the area were gathered through classical fieldwork. Seismic or well data do not exist for this area. Furthermore, a 3D point cloud captured by terrestrial LIght Detection And Ranging (Lidar) technology combined with real-time kinematic global positioning system has been used to complement the geological data and to obtain a virtual 3D digital outcrop model. Following the workflow developed by García-Sellés and described in Geyer et al. (2015), the sequence-stratigraphic analysis and the facies recognition mapped in 2D were transferred to the 3D point cloud (Fig. 7A–B). Combining the facies and sequence-stratigraphic analyses (described in previous sections 2.2 and 2.3) and the 3D point cloud, a conceptual model was established (Fig. 7C) where the main system tracts, bounding surfaces, stacking patterns (aggradation, progradation and retrogradation) and stratal terminations (onlap, downlap and truncation) are highlighted. The 3D point cloud was also used to measure, when possible, the dimensions of the different modelled carbonate sedimentary bodies (mainly FA I and II; Fig. 7C). The conceptual model and the stratal dimensions measured were used for the latter model-data comparison and as a reference model to constraint the most satisfactory simulation (see the summarized key parameters for each

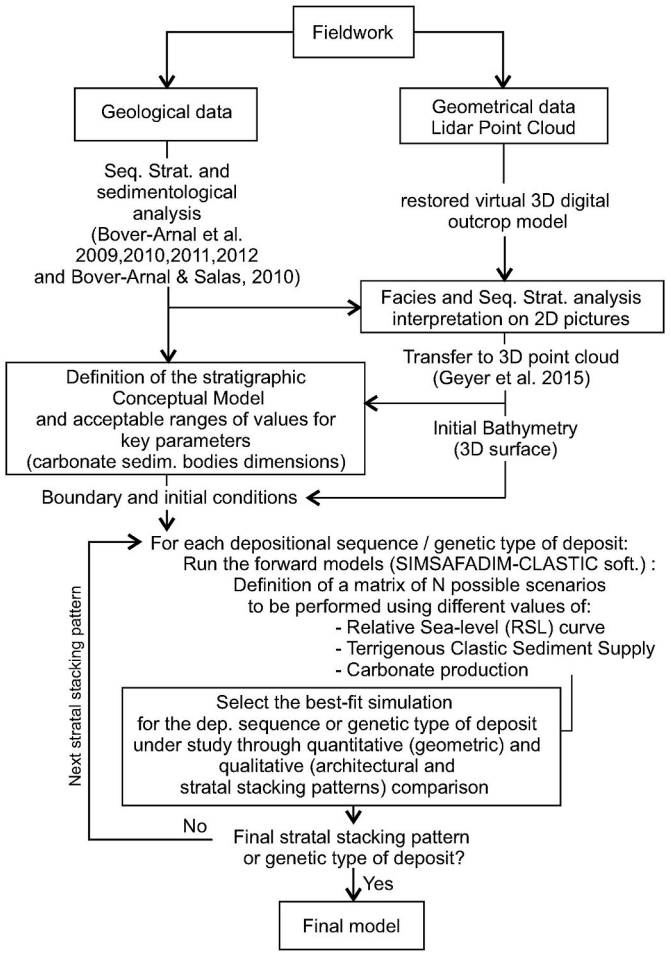

Fig. 6. Workflow followed to build models and assess the relative contribution of carbonate sediment production, clastic sediment supply and the relative sea-level curve (RSL) on the architecture of the platform-to-basin transition domain of Las Mingachas. Simulations are compared to field data through quantitative (geometric) and qualitative (architecture and stacking patterns) constraints. The modelling approach was performed with SF-CL code.

unit in Fig. 7C). To facilitate the architectural and sequence-stratigraphic comparison between the outcrop and the resulting 3D models, two different cross-sections were defined near the areas where well-established parameter values were acquired (cross-sections X and Y; see their location in Fig. 7A–B).

Based on the 3D point cloud and the sequence-stratigraphic and facies analyses obtained from the outcrop interpretation (sections 2.2 and 2.3), a first calibration of the RSL curve was established defining the position of four anchor points (Fig. 4) and measuring the stratigraphic thicknesses between them. The starting point of the modelled succession is located at the base of the platform top limestones of the upper part of Depositional Sequence A and was arbitrarily defined at RSL = 0 m (see location in Figs. 4B and 7C). The second anchor point (RSL = 10 m) coincides with the top of the preserved part of the HNR limestones of Depositional Sequence A that show a stratigraphic thickness of about 10 m (Figs. 4B and 7C). The third point (RSL = −70 m) was set at the base of the FR wedge of Depositional Sequence A (Fig. 7C). The fourth and last anchor point, which is set at >50–60 m, is located above the Maximum Flooding Surface (MFS) of Depositional Sequence B (see Figs. 4B and 7C). This highest anchor point (RSL >50–60 m) was set in function of (i) the stratigraphic thickness between this last stratigraphic position and the first anchor point, and (ii) the estimated water depth for the HNR carbonate platform deposits of Depositional Sequence B. From these four anchor points and considering different time intervals, multiple RSL curves may be possible (see Fig. 7C) and thus, need to be accurately analysed for each modelling sequence to figure out the best-fit curve. Note that for the sake of simplicity, the RSL curve modelled will be discretized in piecewise linear trends instead of curves.

Total simulated time is around 1450 ky and is based on ammonoid biostratigraphy and strontium-isotope stratigraphy (Bover-Arnal et al., 2009, 2016; Moreno-Bedmar et al., 2009, 2010; Garcia et al., 2014) translated to the numerical ages by Gradstein et al. (2004) (see Figs. 3 and 7C), as well as on field data-model best-fit tests carried out with different RSL curves. Although time discretization is done automatically by the program according to the Courant stability criterion avoiding numerical errors (in function of the flow velocity and the spatial discretization) (Steefel and MacQuarrie, 1996), the program outputs are stored every 6 ky for visualization purposes.

Beyond these previous uncertainties including the evolution of the RSL curve and the time of each simulated stage, other key controlling factors such as autochthonous carbonate production rate and terrigenous clastic sediment supply has been considered (see sections 3.5 and 3.6). Therefore, in order to (1) analyse the complex relationship between these controlling parameters and (2) to optimize the modelling workflow, the simulations resulting from the parameter combination have been performed sequentially for each depositional sequence and/or each genetic type of deposit. In this way, the number of simulations performed is less, modelling first Depositional Sequence A and using the resulting basin geometry of the best-fit simulation as the base for the subsequently Depositional Sequence B simulation. In any case, for each group of simulations, a summary and discussion of the results is included for an easier understanding about the effect of each parameter variation on the sedimentary system under study. Additionally, a quantitative and/or qualitative sensitivity test is also included to discuss the relative role of controlling factors on facies distribution, dimensions of carbonate bodies and strata stacking patterns.

3.3. *Modelling limitations and uncertainties*

The modelling approach requires the definition of a certain range of input parameters controlling the processes modelled. As more uncertainties exist, more parameters must be considered, each one tested in an acceptable range of values. As a result, 1) the combination between them increases exponentially the number of the possible geological scenarios, and 2) the selection of the best-fit scenario, and the sensitivity study of each parameter on the final geometry or sediment distribution, becomes more difficult. In function of the geological data available and the numerical model used, some simplifications and assumptions can be applied to constrain the number of possible scenarios and to help the parameter analysis as well.

For simplification purposes and to reduce the number of simulations performed, the number of the controlling parameters considered in this study has been limited to 1) the evolution of the RSL curve and the time of each simulated stage, 2) the autochthonous marine carbonate production rate, and 3) the allochthonous terrigenous clastic sediment entering the basin. Other unknown parameters showing lower percentages although no less important (i.e., lime mud produced or resedimented clastic carbonate, see next section 3.5) have been set fixed and estimated from the existing field data and the literature (when possible).

Finally, in the model runs, no erosion is considered as cannot be modelled by the program in its current version. In addition, the available field and petrographic data do not allow precise corrections for compaction and/or dissolution and thus have neither been included in the model. However, these processes can impact both sedimentary thicknesses and palaeobathymetry evolution, and need to be analysed as new data exists. Regarding to erosional processes and as explained in section 2.3, only the HNR carbonate platform top of Depositional Sequence A was exposed subaerially and partially eroded during the FR stage (Figs. 4 and 7). In this respect, the thickness of the HNR carbonate platform top deposits of Depositional Sequence A has been set at 10 m

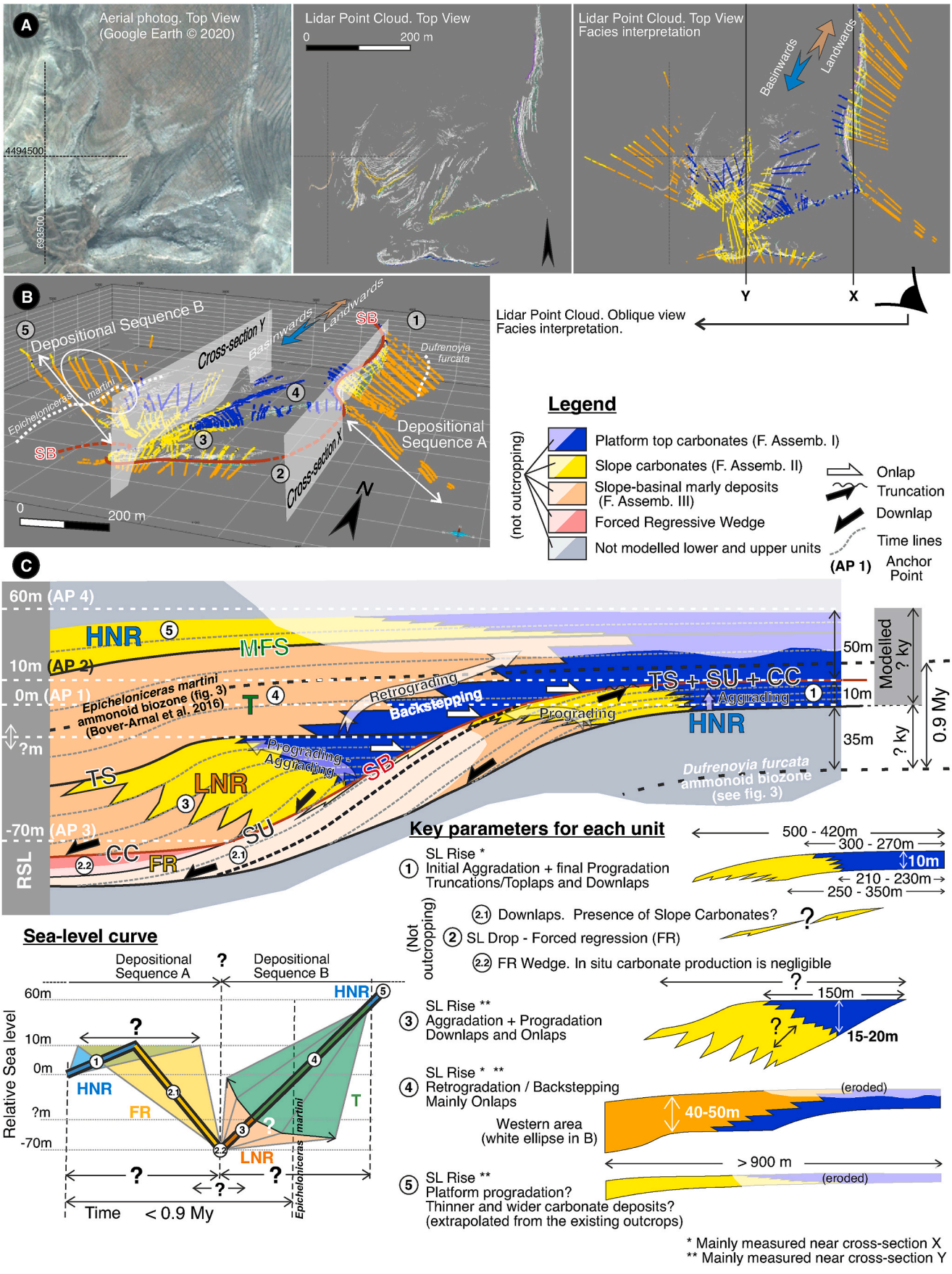

(caption on next page)

Fig. 7. A) Aerial photograph of the studied area, the digital point cloud and the facies interpretation derived from the Lidar acquisition following the workflow described in Geyer et al. (2015). B) 3D oblique view of the digital point cloud in which facies are interpreted (see coloured code). The location of the cross-sections X and Y used to show and compare the model results in the following steps is also indicated. Note the different genetic types of deposit (systems tracts) and the overall facies architecture of the outcrop modelled where platform top carbonates pass basinwards to slope carbonates and basinal marly deposits. The area marked with a white ellipse is discussed in the main text and highlights the occurrence of HNR slope carbonates overlying T basin marls of Depositional Sequence B. C) Conceptual model obtained from field data based in the sequence-stratigraphic interpretation by Bover-Arnal et al. (2009). This conceptual model is used as a reference framework to perform the modelling approach and to establish the key parameters used to constrain the best-fit simulation for each genetic type of deposit. These key parameters include facies architecture, qualitative constraints such as stratal stacking patterns, and the main uncertainties. Note that some parameters have been collected near cross-sections X or Y. The relative sea-level curve (RSL) used in the modelling it is also represented (bottom left image) and includes the estimated elevation from the anchor points (see Fig. 4B and the conceptual model in this figure, marked with *AP*) and its main uncertainties. As a result, a wide range of RSL curves must be tested. See Fig. 4 for abbreviations used in the conceptual model.

(anchor point 2; Fig. 4) as a minimum expected thickness for this unit. The observed truncations due to subaerial exposure at the top of the HNR unit of Depositional Sequence A (see Bover-Arnal et al., 2009, 2010, 2011) cannot be directly simulated with the current version of the program.

3.4. Initial bathymetry and fluid flow system

The modelled area is defined according to the platform margin extension (864 m × 513 m) and discretized in a FE mesh with a spatial resolution of 27 m (Fig. 8). The initial basin topography for model runs corresponds to the base of the HNR platform top and slope carbonates of the Depositional Sequence A set at the first anchor point (Fig. 4). The basal surface was generated and interpolated from the 3D digital virtual outcrop and constrained by the dip attitude of the stratigraphic layers gathered from the fieldwork. This surface was later restored to its original position prior to the Alpine deformation assuming a limb rotation process and taking into account the dip of the initially

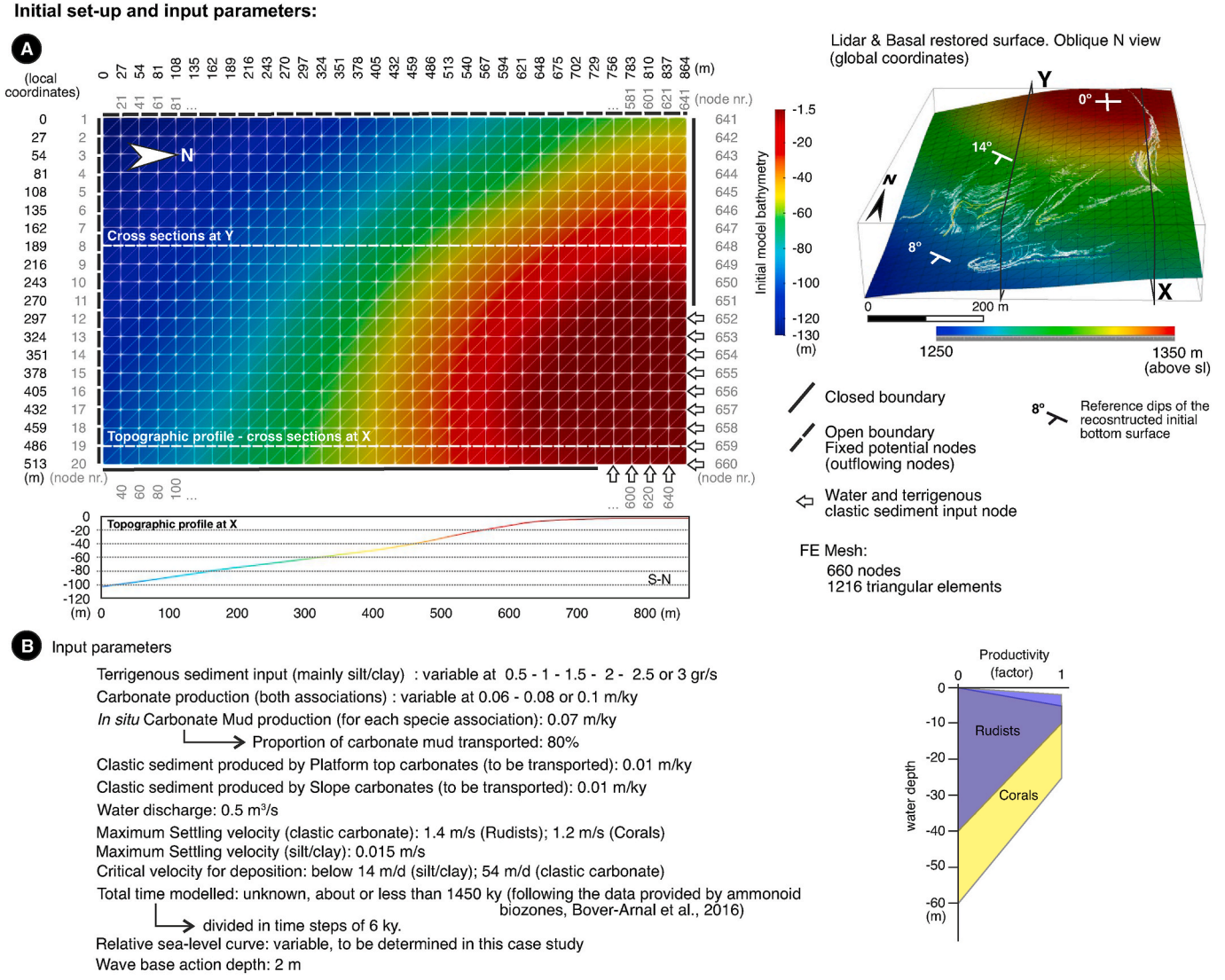

Fig. 8. A) Initial modelling set-up derived from the field and Lidar data (upper right 3D oblique view where the main dips of the surface are included). Finite element (FE) mesh showing the initial bathymetry and boundary conditions used to model the fluid flow system where the initial inflowing and outflowing areas have been defined simulating a mainly N–S trend. See the position of the cross-sections X and Y. The initial topographic profile of the cross-section X is also included. B) Main modelling parameters used in for the studied area for carbonate and clastic sediments.

horizontal surfaces (e.g., the platform top carbonates) that currently are slightly tilted around 9° towards the southwest (Vergés et al., 2020). Thus, the restored surface shows a relatively flat top at the NE corner of the area modelled increasing its dip attitude towards the SW (basinwards) (SW) (see the bathymetry and the dip angles in Fig. 8A). Thus, the initial bathymetry has been set at −1.5 m in the NE corner and at −130 m in the SW corner.

From this initial bathymetry and the facies distribution observed in the field, the model assumes a NNE-SSW transport direction from the platform top area to the basin. As no detailed information exists and for the sake of simplicity, mainly advective transport processes has been considered. Thus, the inflow water discharge area has been defined initially at the NE corner of the modelled area and the outflowing areas at the S and W boundaries of the FE mesh (Fig. 8A). These boundary conditions can automatically be changed by the program depending on the shoreline location due to sea-level variations through time. As no important drainage network exists and a relatively gentle topography is assumed, the water discharge was estimated at 0.5 m^3/s through the inflowing area, to induce a flow system in NNE-SSW direction. Thus, the flow velocities obtained through the basin are in function of the water discharge defined in the inflowing area, the water depth in each point of the FE mesh and the distance from the source area.

3.5. Carbonate production model

As explained in the previous section 2.3, the carbonate production model is set following two main facies associations: Platform top (FA I) and Slope (FA II) deposits. Corals and rudists were the main carbonate producing species in this Aptian example (Bover-Arnal et al., 2009, 2010). For the present modelling, corals and rudists were set to have thrived in water depths ranging between 0 and 60 m and shallower than 20 m, respectively. These depth ranges are in agreement with different palaeoecological models carried out on Aptian carbonate platforms (e.g., Skelton et al., 2010; Bover-Arnal et al., 2012; 2015; Fernández-Mendiola et al., 2013; Gili et al., 2016; Gili and Götz, 2018). The autochthonous maximum carbonate production rate for each species association has been tested with values of 0.06, 0.08 and 0.1 m/ky. Mean values between 0.06 and 0.1 m/ky have been reported for Cretaceous carbonate platforms by Schlager (1981) and James and Bone (1991). Environmental parameters affection (in this case, water depth) on carbonate producing organisms are set through trapezoidal influence functions (Clavera-Gispert et al., 2017) defining the depths with a maximum carbonate production factor. As corals are present in both facies associations and rudists mainly in FA I, the maximum productivity factor (equal to 1) for rudists has been set between −2 and −10 m decreasing linearly until −40 m. While for corals, has been set between −5 and −35 m decreasing linearly until −60 m (Fig. 8B).

The FA III corresponding to basinal marly deposits constitutes a mixture of lime mud (20–60%) and terrigenous silt and clay (40–80%) in different proportions. Thus, in order to model the smallest carbonate fraction induced or produced by carbonate-producing species (mainly calcareous algae and foraminifera), a maximum production rate of lime mud for each species is set at 0.07 m/ky. This production rate is in accordance with the mean value expected from these carbonate-producing organisms (ranging between 0.03 and 0.3 m/ky; see Neumann and Land, 1975; Nelsen and Ginsburg, 1986; Debenay et al., 1999). From the resulting total lime mud produced, 20% is para-autochthonously deposited where carbonate producing organisms live as estimated from field analysis. Furthermore, in order to simulate the lime mud proportion observed in the basinal marly deposits, the remaining 80% of the total amount of lime mud produced is directly transferred to the fluid flow system to be transported basinwards as clastic sediment in suspension mixed with the terrigenous sediments and will be deposited in function of its own depositional parameters (see Fig. 8B). The expected settling velocity and critical velocity for deposition for silt/clay (fraction < 0.002 mm) are < 0.3 m/day and <0.06 cm/s (<51.84 m/day), respectively (Ferguson and Church, 2004).

As no erosional processes can be modelled directly by the program, in order to simulate resedimented clastic carbonates from FA I and II, the program allows to define different carbonate-clastic sediments produced by the reworking of each species association. As no other information exists, this value has been set in function of the proportion of estimated reworked carbonate from field data. Thus, the carbonate-clastic maximum production rate has been set at 0.01 m/ky for each modelled facies association. The carbonate clastics can be entirely transported and resedimented basinwards in function of the fluid-flow system. The main parameters for these carbonate-clastic sediments are summarized in Fig. 8B.

3.6. Terrigenous clastic transport and sedimentation

To the previous lime mud and two carbonate-clastic sediments, a third type of clastic sediment has also been defined to simulate the terrigenous silt/clay proportion contained in the basinal marls (FA III). Given that there is no field data about the amount of allochthonous terrigenous input, this value has been tested between 0.5 and 1–1.5–2–2.5 and 3 gr/s (of silt/clay clastic sediment type) and were estimated in function of the theoretical maximum sediment volume necessary to fill the sedimentary basin (set by the initial bathymetry, the available accommodation, and the amount of time modelled). The input area is also located at the NE corner where the inflowing nodes are defined. Transport and sedimentation parameters for the terrigenous sediment have been set with the same values than carbonate lime mud given that also corresponds to silt- and clay-sized particles (Fig. 8B).

Thus, the total amount of terrigenous sediment deposited in each time step at each node of the FE mesh will be in function of the sediment concentration in suspension and the flow velocity that controls the final settling velocity for each sediment type. Initial conditions established by the program to solve the sediment transport and sedimentation equations are defined considering that the basin has no sediment concentration in suspension at the initial time step. Boundary conditions for sediment and water input has been summarized in Fig. 8A.

4. Modelling results

As mentioned above, the modelling approach has been performed sequentially for each depositional sequence (A and B) combined with the described controlling parameters. Simulation outcomes for each genetic unit modelled have been grouped and outlined below. As the results of the prior genetic type of deposit are constraining the accommodation for the following unit, the best-fit simulation selection is also included at the end of each section. For the sake of simplicity and to facilitate the comparison between model outputs and field data, the following figures only show the facies assemblage obtained for every time step (6 ky) in each node of the FE mesh.

4.1. Depositional sequence A. HNR and FR genetic units

For the first depositional sequence considered, a rising (HNR) and falling (FR) relative sea-level stages are modelled. The initial (0 m), middle (10 m) and final RSL elevation (−70 m) are inferred from the field data (see anchor points in section 3.2 and Fig. 4), but the time when each position is reached remains unknown. This fact sets the shape of the RSL curve and consequently the falling and rising rates. Thus, for modelling purposes and to simulate both RSL stages, 22 different RSL curves were tested with turning points when the RSL reaches the highest (HSL) and lowest (LSL) positions (see Fig. 9). The total time modelled for the HNR and FR units of Depositional Sequence A has been tested between 258 and 402 ky.

Every RSL curve has been combined with three different autochthonous maximum carbonate production rates (0.06, 0.08 and 0.1 m/ky) and six different amounts of inflowing clastic terrigenous sediments

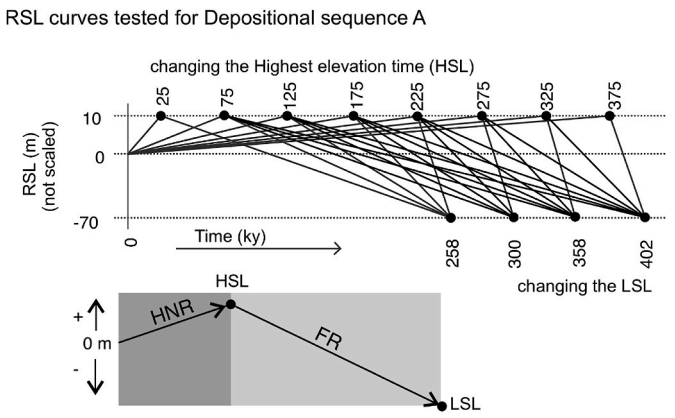

Fig. 9. Relative sea-level curves (RSL) tested for Depositional Sequence A where a relative sea-level rise and fall is expected from field data analysis belonging respectively to a HNR and a FR. The initial RSL elevation has been set at 0 m. Different sea-level rising or falling rates have been tested (22 distinct RSL curves in total) changing the time when the sea level reaches its highest elevation (HSL) at 10 m, and its lowest elevation (LSL) at −70 m.

(0.5, 1.0, 1.5, 2.0, 2.5 and 3.0 gr/s) that outputs 396 different scenarios for Depositional Sequence A. To show the effect of one of the tested controlling parameters on the geometry and evolution of each facies assemblage, only the simulations with equal values for the other two parameters have been analysed. The simulation outcomes have been summarized in Fig. 10 and are described below. As the dimensions for each carbonate deposit studied have been measured at the NE part of the area modelled, cross-section X was used to show and to compare the results (see location in Fig. 7A–B).

4.1.1. Effect of the RSL curve

To show the effect of changing the RSL curve on stratal stacking patterns and facies distribution, only those simulations defined with the same autochthonous maximum carbonate production rate and terrigenous supply (e.g., 0.08 m/ky and 2.0 gr/s, respectively) have been compared. As it can be observed in Fig. 10A, the relative time when sea level reaches its highest elevation (HSL) strongly influences the system in the following ways: (1) the thickness of both HNR and FR units, being thicker or thinner with lower or higher sea-level rise or fall, respectively; (2) the stacking pattern of the FA I during HNR, changing from retrogradation (fastest sea-level rise, HSL = 25 and 75 ky), to aggradation (HSL = 125 ky) and progradation (HSL > 125 ky); (3) the progradation rate and distance of the FA II, being greater when sea level rises slowly; (4) the presence of carbonate deposits in the FR unit, being greater with faster sea-level drops where only FA II grows (HSL ≤ 225 ky); (5) the total amount of sediment deposited, being greater as sea level rises slowly given the maximum carbonate production rate recorded under optimal conditions over a longer time, as well as the greater accommodation available (Fig. 10A with a HSL from 25 to 225 ky simulates the same amount of time); and (6) the resulting geometry of the sedimentary body generated due to a more proximal (e.g., HSL = 225 ky) or distal (e.g., HSL = 25 ky) sedimentation of terrigenous materials. Proximal sedimentation also favours optimal conditions for carbonate production in the proximal areas near the platform edge and as a result, the system is forced to prograde. Note that considering a fast sea-level rise (between HSL at 25 and 75 ky, and LSL at 258 ky) opposite stacking patterns are obtained for the FA I and II, showing retrogradation for the FA I and progradation for FA II.

4.1.2. Effect of the rate of RSL drop

To study the effect of the rate of RSL drop on the FR unit geometry and facies distribution, simulations with the same terrigenous input rate, autochthonous carbonate production and HSL (e.g., 2.0 gr/s, 0.08 m/ky and 175 ky, respectively) were considered. The changing parameter between each simulation is the time when the RSL reaches the lowest elevation (LSL ranging from 258 to 402 ky), simulating different rates of RSL fall (Fig. 10B). Under these conditions, the main differences are visible in the FR unit during the RSL drop stage increasing the sediment deposited as decreasing the RSL drop rate due to the increase of the total-time modelled (from 258 to 402 ky). Regarding to FA distribution, only the FA II is present in the FR stage and shows an almost the same or slightly lower extension in the considered simulations as decreasing the rate of RSL fall. The HNR unit during the stage of RSL rise remains constant as all the considered simulations under these conditions follow the same rising rate.

4.1.3. Effect of autochthonous carbonate production

The effect of changing the rate of autochthonous carbonate production can be established from those simulations with identical terrigenous sediment input rate (e.g., 2.0 gr/s) and the same RSL curve, for instance 0–175–258 ky (Fig. 10C). The increase on the carbonate production rate ranging from 0.06, to 0.08 and to 0.1 m/ky allows to increase the progradation rate during both stages of RSL rise and fall. The most sensitive facies association is the FA II, which significantly expands as carbonate production rate increases. During the FR stage, only FA II and III are present.

4.1.4. Effect of terrigenous clastic supply

The changes produced by different clastic terrigenous sediment input (set at 0.5, 1.0, 1.5, 2.0, 2.5, and 3 gr/s) can be observed comparing those simulations with equal carbonate producing rate (e.g., 0.08 m/ky) and the same RSL curve (e.g., 0-175-258 ky) for each inflowing sediment considered. Under these conditions the increase of inflowing terrigenous clastic sediment (Fig. 10D): (1) allows to increase the total sediment deposited changing the geometry of the sedimentary bodies from tabular to sigmoidal; (2) FA I changes its progradation rate although it does not follow a linear relationship; (3) FA II (the most sensitive FA) decreases its basinward extension and width, and changes the stacking pattern from mainly aggradation to progradation; and (4) the carbonate lime mud proportion contained in FA III is lesser due to sediment input increase and a lower carbonate production.

4.1.5. Selecting the best-fit simulation for the depositional sequence A

For this depositional sequence, 396 different scenarios were obtained. To reduce the number of potential scenarios the following criteria were considered: (1) the geometric constraints for sequence A are mainly measured along the HNR unit (Fig. 7C), (2) there are no geometric constraints for the FR unit given that it corresponds to a metric bed cropping out in 2D (Fig. 4), and (3) the HNR unit is strongly influenced by the rate of RSL rise (see section 4.1.1), while the rate of RSL fall has no significant effects on the resulting facies and stratigraphic architectures (see section 4.1.2). Therefore, the simulations with different rates of RSL drop can be ruled out thus reducing from 396 to 144 the number of simulations to be compared.

As mentioned in section 3, the geometric and architectural properties used to compare the model output and the field observations (Fig. 7C) are: (1) the thickness of the HNR platform top carbonate unit (FA I), (2) the minimum and maximum basinward extension of the platform top and slope carbonate deposits (FA I and II), and (3) the expected stacking patterns for both FA I and II (only progradation can be accepted as shown in Fig. 7C). The selection of the best-fit simulation has been conducted by plotting the differences between the measured five constraints and the simulation outcomes for each model run (Fig. 11A). Note that concerning field geometric data ranging between two different values (e.g., maximum extension of FA II), the mean value has been used for comparing purposes. Thus, simulations showing retrogradation and/or only aggradation for at least one FA, or/and dimensions greater than 10% above or below those measured in the field, were rejected (grey shaded areas in Fig. 11A) reducing considerably the number of possible

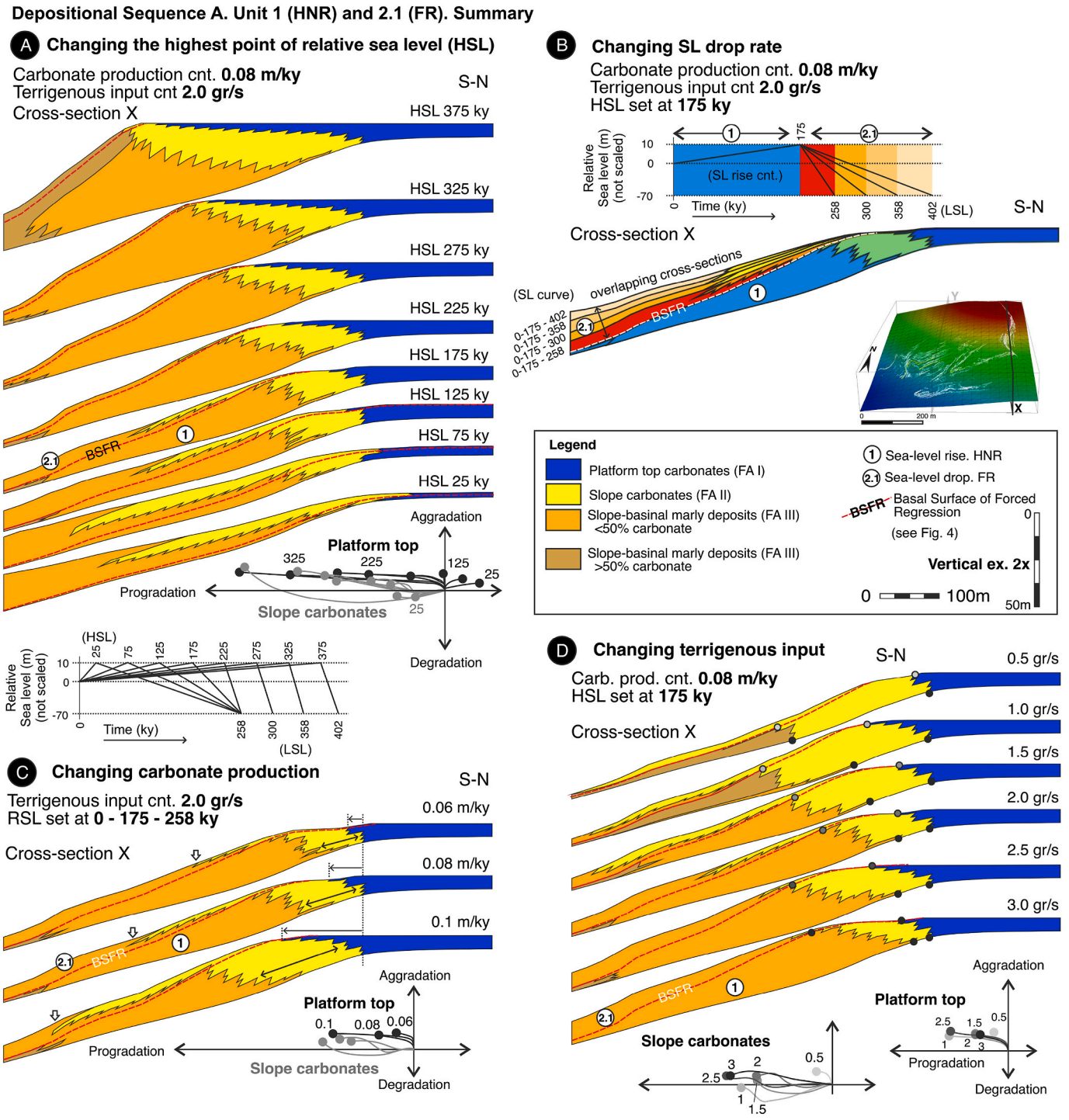

Fig. 10. Summary and comparison of models obtained for Depositional Sequence A along the cross-section X (see its location in Fig. 7 and in this figure's 3D oblique view) where the main key parameters for this sequence are measured. The Basal Surface of Forced Regression (BSFR) is included in all the simulation results. See main text for a more detailed explanation. A) Effect of the sea-level curve used, which is characterized by the time of the highest elevation of relative sea level (HSL). Maximum autochthonous carbonate production and clastic terrigenous supply are fixed at 0.08 m/ky and 2.0 gr/s, respectively. The migration diagram of the carbonate facies during the RSL rise stage is also included. B) Effect of the sea-level drop ratio fixing the HSL and changing the length of the forced regression changing the time when the RSL reached its lowest elevation (LSL). The first rising stage produces the same stratigraphic record while the second one (2.1) is thicker as the length of the forced regressive stage increases, but the facies distribution remains almost constant. C) Compared changes on the rate of maximum carbonate production with a fixed clastic terrigenous supply (2.0 gr/s) and the same RSL trend (0-175-258 ky). Note the aggradation-progradation and mainly progradation stacking patterns displayed by the migration diagram for the platform top and slope carbonates, respectively, when carbonate production rates increase. The slope carbonates also show a wider development and increase their extension during the sea-level drop (see white arrows). D) Effect of changing the terrigenous sediment input while the maximum autochthonous carbonate production remains constant (0.08 m/ky) and the RSL curve is set at 0-175-258 ky. The migration diagram of the carbonate facies during the RSL rise stage it is also included to show the effect of the siliciclastic input on the aggradation-progradation trend. Note that the width of the slope facies is decreasing while increasing the siliciclastic sediment supply.

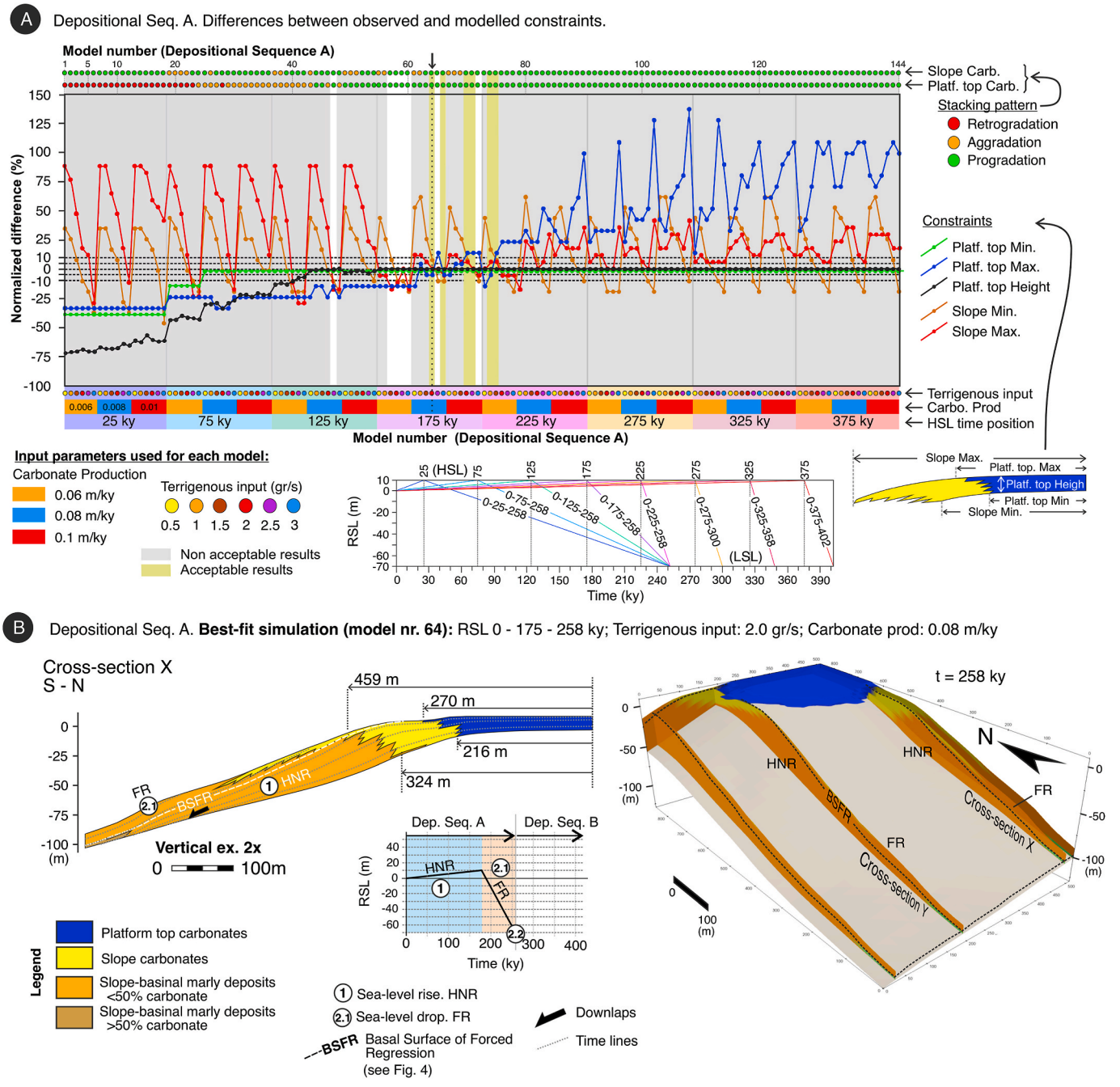

Fig. 11. Best-fit simulation for Depositional Sequence A. A) Difference between the expected and the modelled dimensions for the platform top and slope carbonate facies assemblage for each model run for Depositional Sequence A. The difference has been plotted using the normalized value for each measurement (in %). The input parameters combination (the RSL curve defined by its higher position HSL in the bottom of the image, the maximum autochthonous carbonate production and the clastic terrigenous sediment supply) results in 144 different models (see the colour legend inset). For each RSL curve, 18 models have been analysed. The sacking pattern for the platform top and slope facies has been also plotted at the upper part of the graph (see coloured dots and the corresponding legend). Note that the best-fit simulation is marked with a black arrow showing differences between the expected and obtained dimensions near 0%. Other slightly inaccurate but with acceptable results are also highlighted with a light-green rectangle. B) Cross-section X showing the selected best-fit simulation for Depositional Sequence A derived from the analysis of the previous plotted dimension differences. The selected simulation belongs to a RSL curve changing its elevation from 0, 10 and −70 m at 0, 175 and 258 ky, respectively. Terrigenous supply is set to 2.0 gr/s and maximum autochthonous carbonate production rate to 0.08 m/ky. A 3D fence diagram it is also included in the 3D oblique view. The platform top carbonate sedimentary body prograding basinwards has been also represented in 3D. (For interpretation of the references to colour in this figure legend, the reader is referred to the Web version of this article.)

simulations. Therefore, only few models match the key parameters within an acceptable difference range (e.g., all parameters below 10% or one slightly above 10%) and a proper stacking pattern for both FA I and II (highlighted by a light-green area in Fig. 11A). Only one model best-fits field observations and interpretations showing errors below 10% (number 64, black arrow, Fig. 11A). This best-fit model was set by a RSL curve of 0–175–258 ky, a carbonate production rate of 0.08 m/ky and a rate of inflowing terrigenous sediments of 2.0 gr/s (Fig. 11B). Other similar, but slightly worse results for FA I are obtained increasing the carbonate production rate to 0.1 m/ky. Changing the RSL curve to 0–225–258 ky, the rates of carbonate production and terrigenous supply need to be set to 0.06 m/ky and 1.0 or 1.5 gr/s, respectively, to obtain

more or less acceptable results.

Another aspect that can be stated quantitatively from the analysis of the plotted differences (Fig. 11A) but also qualitatively from the results comparison (Fig. 10), is that, the final facies distribution and dimensions results from the combination of all controlling parameters (as stated also in Catuneanu, 2020) but in different weights. In this regard, the initial elevation and fluctuations of RSL mainly control the location where carbonate deposits develop and their overall geometry. On the other hand, changes in terrigenous input and carbonate production may also exert control on the resulting facies architecture. For example, FA II is the most sensitive assemblage to such variations (note the dispersion in red and brown lines in Fig. 11A when the inflowing terrigenous sediment or the carbonate production rate change regardless of the RSL curve used). In contrast, the platform top facies (FA I) shows a high dependency on inflowing terrigenous clastics but only with lower rates of RSL rise (blue line with higher values of HSL; Fig. 11A). This fact is a consequence of increasing the terrigenous inputs combined with low rates of RSL rise that results in a basinward extension of the prograding system due to an increase of the basin area with optimum water depths.

From the final selected scenario that best fits the field data (Fig. 11B), some parameters can be used as a reference to continue with the simulation process of Depositional Sequence B. However, and focused on the FR unit, other related RSL curves with the same HSL at 175 ky but with a different amount of time modelled (different LSL) can also be considered (e.g., 0-175-300 or 358 or 402 ky, see Fig. 10B). More available geological data from this basin-floor wedge would help to constrain other possible geological scenarios for the upper FR unit. However, with the existing field data and for simplicity, the basin geometry obtained at the end of Depositional Sequence A, which considers a RSL curve set at 0-175-258 ky, was used as a reference for the initial bathymetry of Depositional Sequence B, as well as for the final RSL time and elevation.

4.2. Depositional sequence B. Modelling approach and initial considerations

Modelling of Depositional Sequence B includes three different genetic units described in section 2.3: a Lower Normal Regression (LNR), a Transgression (T) and the subsequent HNR (see Figs. 4 and 7C). For the sake of simplicity, the LNR and T were simulated independently from the HNR. As stated in the previous section 3, only the initial (−70 m) and final (60 m) RSL elevation can be estimated from field data for Depositional Sequence B (anchor points 3 and 4; Fig. 4), but no other information about the intermediate RSL elevation can be deciphered. Thus, the main uncertainties to simulate Depositional Sequence B are: (1) if the rate of RSL rise is constant following a straight-line, or (2) if the rate of RSL rise needs to change to reproduce the stages of LNR, T and HNR, (3) if so, the time and elevation of this change, (4) the total simulated time for this depositional sequence, and (5) if the rate of terrigenous clastic input remains constant and equal to the previous depositional sequence. Modelling approach follows the same procedure as described for the prior depositional sequence, meaning that different RSL curves were tested changing the time and the elevation of a point of inflection between each genetic unit or changing the final time step. Using all possible RSL curves derived from the proposed points of inflection between each genetic unit results in a large number of simulations (Fig. 12). For this reason, the simulation process for Depositional Sequence B has been optimized following a sequential approach for each genetic unit (Fig. 12B) instead of trying to model all the units together (Fig. 12A). Thus, the RSL best-fit curve (and also the basin geometry) obtained for the prior genetic unit is used to test the new RSL curves for the next genetic unit, reducing substantially the final number of simulations performed (see Fig. 12B).

Under these considerations, and taking into account the proposed inflection points defining different RSL curves, finally, for Depositional Sequence B, only 39 different RSL curves were tested (see Fig. 13A for the LNR unit, Fig. 14A for the T unit, and Fig. 15A for the HNR unit) that were also combined with different rates of inflowing terrigenous sediments: 2.5, 2.0, 1.5 and 1.0 gr/s. In order to minimize the number of the

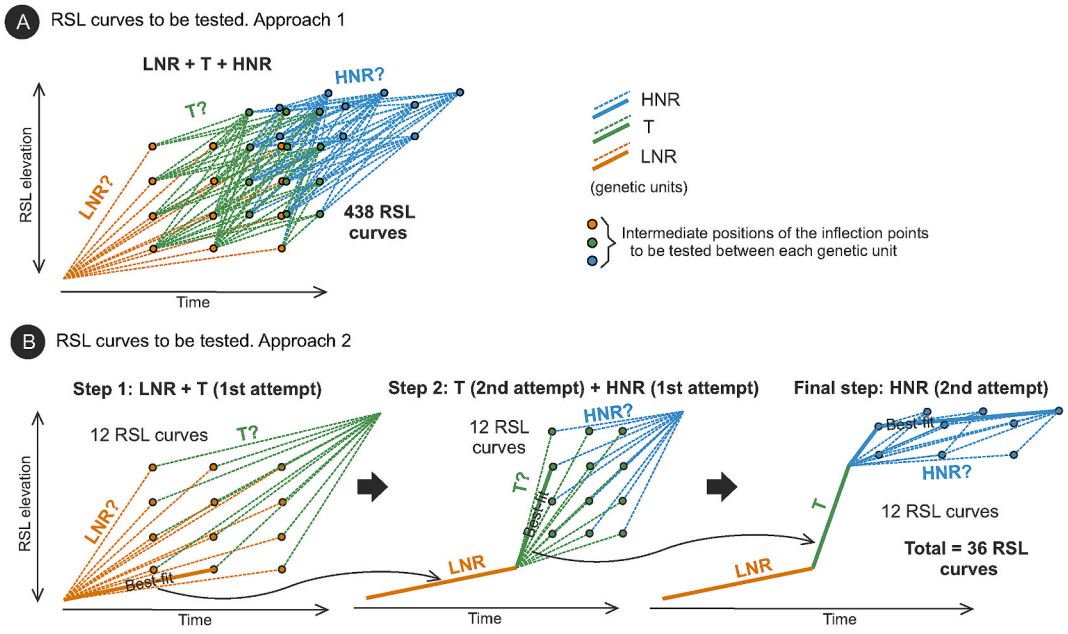

Fig. 12. Conceptual schemes of two different approaches to generate possible RSL curves to be tested. The schemes take into account different unknown intermediate RSL positions, which simulate the expected systems tracts. A) First approach: Combining all the possible intermediate RSL positions together resulting in 438 different RSL curves to be tested. B) Second approach: In this case, the same intermediate RSL positions are combined separately for each expected genetic unit in 3 different steps and, as a result, only 36 different RSL curves are tested. Note that in these conceptual sketches, the ideal intermediate RSL positions are less than those used in the modelled area.

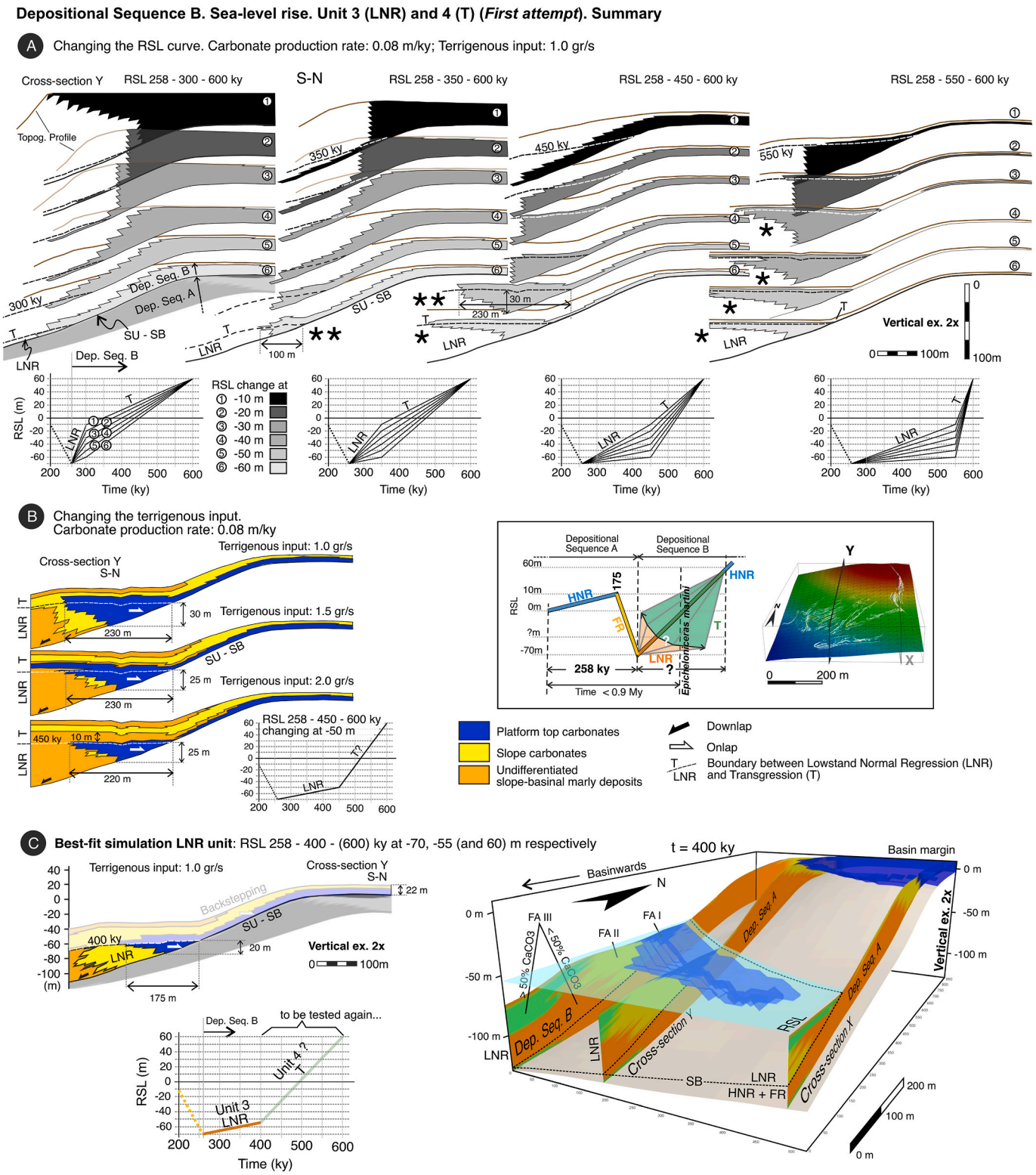

Fig. 13. Summary and comparison of the results obtained for units 3 (LNR) and 4 (T) belonging to Depositional Sequence B. A) Development of units 3 and 4 tested against different RSL curves (see plots below). B) Development of units 3 and 4 tested against different rates of clastic terrigenous supply (1.0, 1.5 and 2.0 gr/s), and compared with those simulations with the same RSL curve 258-450-600 ky that changes the rise rate at −50 m (see the corresponding plot). Considering the results from Depositional Sequence A, maximum autochthonous carbonate production rate is fixed al 0.08 m/ky for all model runs. Note that in this case the cross-section Y has been used to show the results (for cross-section location see 3D oblique view and Fig. 7) and only the platform carbonates (in black-to-grey colours and marked form 1 to 6) are delineated in A. C) Cross-section Y for the selected best-fit simulation (mainly for the LNR succession) and a 3D view of a fence diagram for the modelled successions of the HNR and FR of Depositional Sequence A, and the LNR of Depositional Sequence B. (For interpretation of the references to colour in this figure legend, the reader is referred to the Web version of this article.)

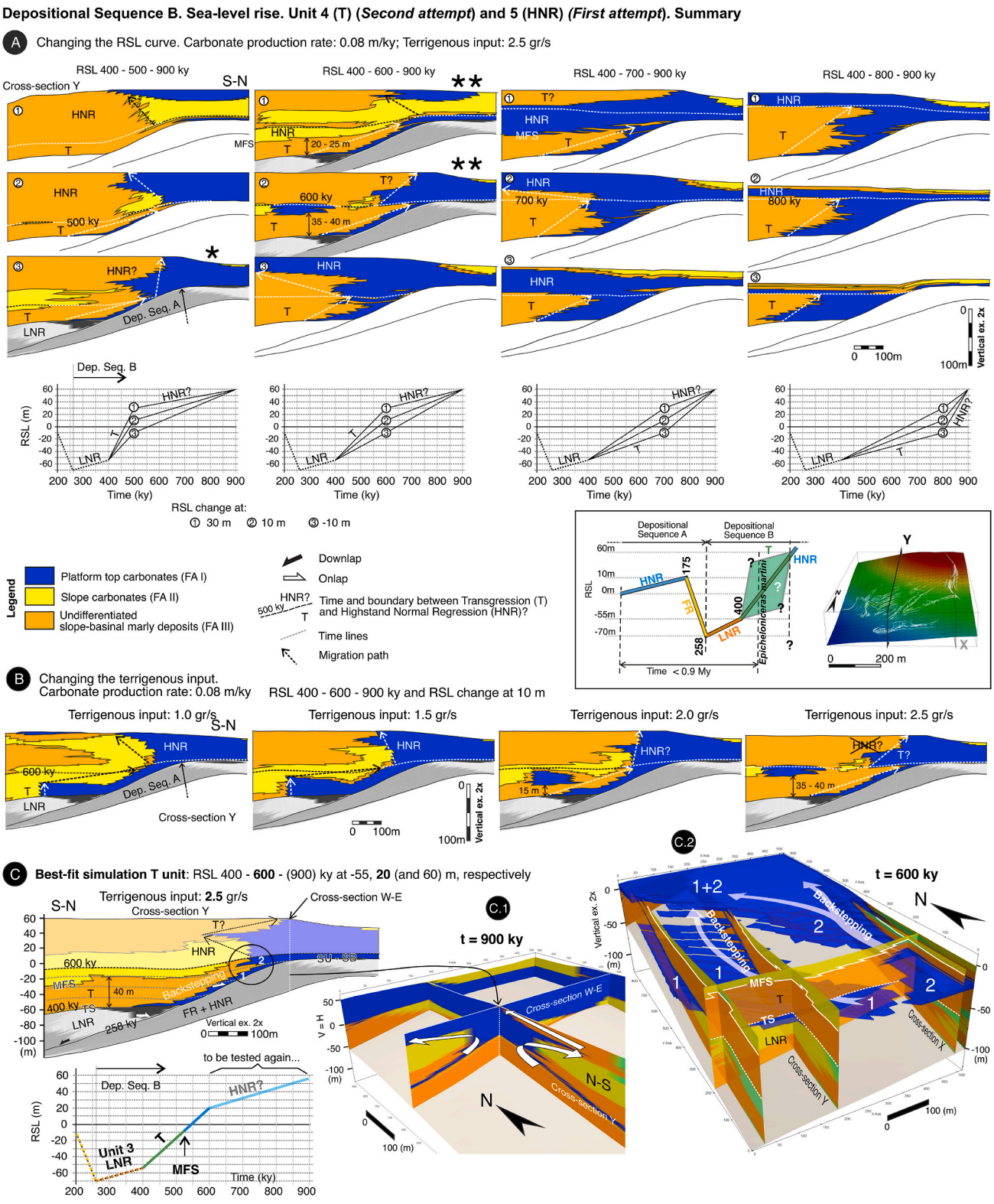

Fig. 14. Summary and comparison of the results obtained for the upper part of Depositional Sequence B including units 4 (T) and 5 (HNR). A) Development of units 4 and 5 tested against different RSL curves (see plots below), which change the time and the elevation of the intermediate RSL position (note that simulations are grouped by the time step when this change occurs). B) Development of units 4 and 5 tested against different rates of terrigenous clastic supply (1.0, 1.5, 2.0 and 2.5 gr/s), and compared with those simulations with the same RSL curve 400-600-900 ky that changes the rise rate at 10 m. Considering the results from Depositional Sequence A, maximum autochthonous carbonate production rate is also set al 0.08 m/ky for all model runs. Cross-section Y has been used to show the results (cross-section location is shown in the upper 3D oblique view and in Fig. 7). The migration path for the platform top facies assemblage is also included to show the apparent stacking pattern obtained. C) Cross-section Y for the selected best-fit simulation and two different 3D views at 600 ky (C.1) and 900 ky (C.2).

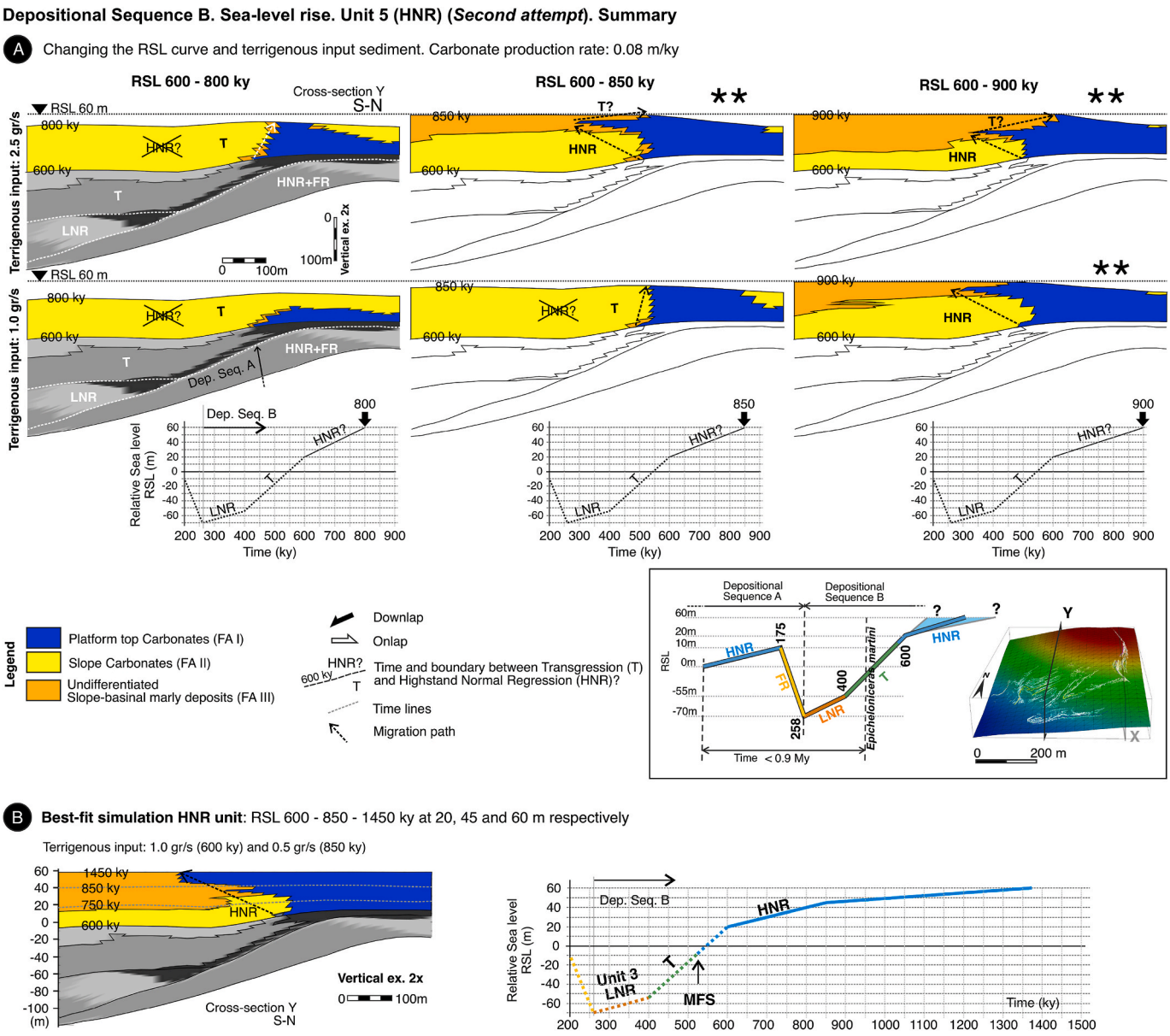

Fig. 15. A) Summary and comparison for the second modelling attempt of the HNR of Depositional Sequence B. This modelling takes into account 3 different RSL curves (lower plots) that change its rising rate by modifying the final time step tested against 2 different inflowing clastic terrigenous sediment rates (1.0 gr/s lower cross-sections, and 2.5 gr/s upper cross-sections). Cross-section Y has been used to show the results (see location of the cross section in the 3D oblique view and in Fig. 7). The last RSL elevation has been also included as a reference at 60 m. B) Cross-section Y for the best-fit simulation of the HNR of Depositional Sequence B setting a rate of RSL rise that decreases at 850 ky. Inflowing clastic terrigenous rate also decreases from 1.0 to 0.5 gr/s at 850 ky. Note the aggrading-prograding stacking pattern obtained for the modelled strata.

simulations performed, the maximum autochthonous carbonate production rate was fixed and set at 0.08 m/ky as is the best-fit value obtained for the prior Depositional Sequence A (if best-fit simulations would not have been obtained for Depositional Sequence B, other possibilities would have been tested). Then, the combination of the proposed values for each controlling parameter for each genetic unit finally results in 126 simulations or possible scenarios for this depositional sequence that can be studied.

A detailed description and the effect of each controlling parameter on each simulated genetic unit are included and summarized in the following sections. For simplicity purposes, the description of the effect of each controlling parameter on the first attempts of the T and HNR units (that were rejected) are not included in the text, but have been illustrated in the corresponding figures (Figs. 13A and 14A for the first attempt of the T and HNR units, respectively) as have been simulated together with the corresponding prior genetic unit. Conversely, the key features used to reject the first attempt have been also included in the best-fit selection process.

4.3. Depositional sequence B. LNR (and T unit, 1st attempt)

Regarding the LNR unit, the quantitative and architectural constraints were set along the cross-section Y (see location in Fig. 7) where the main values were measured. These constraints correspond to (Fig. 7C): (1) an aggrading-prograding stacking pattern for the platform top carbonate deposits, (2) an extension and thickness of the platform top carbonates (FA I) of 150 and 15–20 m, respectively, (3) landwards onlap stratal terminations onto the sequence boundary (SB) and basinwards downlapping clinoforms over the FR unit and onto the correlative conformity (CC) of the SB, and (4) a basinwards lateral facies change

from platform top facies (FA I) to slope deposits (FA II) with unknown dimensions for the LNR unit. For the transgressive unit (T) less constraints exist, and the main ones are (Fig. 7C): (1) FA I is stacked towards the land in a retrograding fashion, (2) FA I evolves basinwards and upwards to basin marls (FA III) with a thickness of 40–50 m, at least, in the western area (white ellipse in Fig. 7B and cross-section Y), while in the eastern part of the area modelled the T unit is actually eroded, and (3) the total simulated time must be long enough to force the T unit to overlie the FA I deposits of the former HNR unit of Depositional Sequence A.

4.3.1. LNR unit: effect of the RSL curve

The effect of the RSL curve used was determined comparing the examples with the same rate of terrigenous clastic supply (e.g., 1.0 gr/s) and autochthonous carbonate production (0.08 m/ky). As the main geometric and architectural constraints were acquired from platform top deposits (FA I), this facies assemblage has been displayed in Fig. 13A with different black-to-grey colours. Simulations are grouped in function of the relative time at which the system shifts from LNR to T (e.g., sea-level changes its rising rate) and taking into account six different elevations where this change occurs (between −60 and −10 m). Under these premises, the mean features that can be highlighted are: (1) the stratigraphic thickness of each unit is inversely proportional to the rate of RSL rise, (2) increasing the duration of the LNR or T stages, sediment thickness increases as well, (3) the total sediment deposited is greater when the change of the RSL rise rate is defined earlier, (4) likewise, thicker FA I deposits are obtained landwards indicating an earlier shift of the RSL rise rate (note that no FA I developed on top of the FA I of Depositional Sequence A with a RSL 258-550-600 Ky and elevations above −30 m), and (5) different stacking patterns for the same FA are obtained changing the intermediate RSL elevation, or changing the relative time when this change occurs.

4.3.2. LNR unit: effect of terrigenous supply

The simulations defined with the same RSL curve (e.g., 258-450-600 ky and a RSL change at −50 m) and autochthonous carbonate production (already fixed at 0.08 m/ky for this depositional sequence), were used to characterize the effect of the three different rates of terrigenous inputs considered (2.0, 1.5 and 1.0 gr/s, Fig. 13B). Regarding the LNR unit, both FA I and II show an aggrading-prograding stacking pattern in the selected simulations. As can be noticed in Fig. 12B, the major difference is the progradation distance and the thickness of both carbonate facies assemblages that increases as terrigenous supply decreases. The most sensitive facies is FA II (slope carbonates) showing substantial differences between terrigenous inputs of 1.0 and 2.0 gr/s.

4.3.3. Selecting the best-fit simulation for the LNR unit (dep. Seq. B)

Bearing in mind the architectural and geometric constraints for the LNR and T units previously defined, and related to the effect of the terrigenous supply, a single best-fit model cannot be selected for both units together using the same RSL curve (Fig. 13B). In this sense, the LNR unit shows better facies distributions and platform dimensions with lower rates of terrigenous supply (1.0 gr/s). On the contrary, the T unit shows better results with higher rates of terrigenous supply (2.0 gr/s) where basinal deposits (FA III) overlay the platform top deposits (FA I) of the LNR unit. However, in this case, the thickness of the T unit is less than the expected (10 m instead of 40–50 m, see Fig. 13B).

On the other hand and related to the RSL curves, only few models show a prograding stacking pattern for the FA I during the LNR stage (marked with * and ** in Fig. 13A) and only two outputs show dimensions ranging between the expected ones (RSL 258-350-600 ky and −60 m, and RSL 258-450-600 ky and −50 m, both highlighted with **), indicating that the best-fit simulation should be obtained setting values between both solutions. In addition, and related to the T unit, the satisfactory models for the LNR stage although output reasonable stacking patterns, show unreliable facies distributions and sedimentary thicknesses below the expected ones (around 20 m), indicating that the total time modelled needs to be at least greater than 600 ky.

Accordingly, from the simulation outputs obtained, only the LNR unit matches some of the simulated parameters including a terrigenous supply of 1.0 gr/s and a RSL curve (only for the LNR stage) starting at −70 m (258 ky) and ending at −55 m (600 ky) (Fig. 13C), which is an intermediate elevation between the previous simulations (** in Fig. 13A). The expected T genetic type of deposit does not fit the tested values and must be simulated again leastways changing the rate of terrigenous supply from 1.0 gr/s to a higher one (≥2.0 gr/s) and defining further RSL curves.

In the 3D oblique view (Fig. 13C), it can be observed how the platform top carbonates (FA I) of the HNR unit of Depositional Sequence A are distributed in a E-W trend parallel to the basin margin and how they thin westwards (and basinwards) as the basin deepens (Figs. 11B and 13C). After the fall in RSL, during the initial rising stage, the FA I of the LNR unit of Depositional Sequence B migrates westwards and shows a WNW-ESE trend parallel to the new coastline and thins eastwards. This unit is currently eroded near cross-section X (Fig. 13C).

For these genetic units less geometric constraints exist. Consequently, a qualitative instead of a quantitative sensitivity analysis was performed from the modelling outputs. Thus, and as stated from the previous sequence, the most sensitive carbonate facies assemblage remains the FA II, which is conditioned by the rate of inflowing terrigenous (Fig. 13B). On the other hand, the dimensions of the FA I are also conditioned by the terrigenous input while the initial platform location and the resulting stacking pattern are strongly conditioned by the rate of RSL rise (for instance, see the unexpected stacking pattern generated when the decrease of the rate of RSL rise is set at −10 or −60 m but at the same time step of 300 ky, Fig. 13A).

4.4. Depositional sequence B. T unit (2nd attempt) and HNR (1st attempt)

The T genetic type of deposit needed to be simulated again following the same procedure in order to explore new possible values for the controlling parameters, in this case: (1) the RSL curve, (2) the total time modelled, and (3) the terrigenous supply. Following this T unit, the subsequent HNR unit was also modelled as a first attempt.

Related to the RSL curve and the time modelled, the initial RSL elevation is set at −55 m (400 ky) from the previous modelled succession, and the last elevation at 60 m (anchor point 4; Figs. 4) and 900 ky as a first attempt. The intermediate elevation of the RSL curve has been tested at different elevations (−10, 10 and 30 m) and the time steps considered are 500, 600, 700 and 800 ky in order to simulate again a change in the rate of RSL rise trying to model the transition between the T and HNR. In this regard, 12 different RSL curves were tested (Fig. 14A). Note that in function of the time and the elevation of the inflection point the resulting RSL curve can be assumed as a straight line with a constant rate of rise (e.g., RSL 400-700-900 ky curve nr. 2, or 400-600-900 ky curve nr. 3; Fig. 14A). Similar curves output almost the same stratigraphic and facies architectures if are following a straight line.

As for the previous modelled unit, autochthonous carbonate production rate is fixed at 0.08 m/ky. Terrigenous supply is tested considering greater values than for the LNR unit as stated from the previous simulations performed during the first attempt. Accordingly, values ranging between 1.0 and 2.5 gr/s were considered (Fig. 14B). The combination of all tested controlling parameters resulted in 48 possible simulations. The architectural and the geometric constrains for the T unit are described in Fig. 7C and in the previous section 4.3. On the other hand, fewer constraints exist for the HNR of Depositional Sequence B due to the poorer outcropping conditions and the present-day erosion. Thus, and as explained in section 3 and summarized in Fig. 7C, from the outcrops located westwards, a prograding stacking pattern and a stratigraphic thickness of around 40–50 m are expected for the HNR unit of Depositional Sequence B.

4.4.1. Unit T: effect of the RSL curve

With fixed rates of terrigenous supply (2.5 gr/s) and autochthonous carbonate production (0.08 m/ky), the influence of RSL can be determined (Fig. 13A). Thus, the main features that can be stated are: (1) the stratigraphic thickness of each unit is inversely proportional to the rate of RSL rise, (2) the platform top carbonates (FA I) of the lower T unit only overlie the FA I of the HNR of Depositional Sequence A when the change of the RSL rise rate occurs above 10 m (field constrains indicate that the FA I belonging to the T unit must overlie the former HNR near the platform top), (3) a retrograding stacking pattern is recorded in the lower part of the interval simulated in almost all the scenarios, (4) in the upper part of the interval modelled, almost all simulations show an apparent prograding stacking pattern, and (5) only three scenarios (marked by * and ** in Fig. 14A) show the drowning of the lowstand platform buried by marly basinal deposits (FA III) that evolve upwards to slope-platform carbonates (FA I and II), and only two simulations (**) display the T unit overlying the platform top carbonates of the HNR of Depositional Sequence A.

4.4.2. Effect of terrigenous supply

In order to characterize the effect of the terrigenous supply on facies distribution and taking in mind that autochthonous carbonate production rate is already fixed (0.08 m/ky), simulations with the same RSL curve and changing the rate of terrigenous supply have been considered (Fig. 14B). Under these conditions, it can be stated that when increasing the rate of inflowing terrigenous clastic sediments: (1) the accumulation of carbonate sediments decrease, (2) the thickness of the marly basinal deposits (FA III) increases for the lower part of the interval modelled below 600 ky, (3) also for this part of the interval simulated the stacking pattern shifts from aggradation/retrogradation to a clear retrogradation, (4) a change from progradation/aggradation to retrogradation in the upper modelled part (above 600 ky) in which apparently no HNR or T units are recorded with rates of inflowing terrigenous equal or greater than 2.0 gr/s, and (5) a new disconnected carbonate platform flourishes in the middle stratigraphic succession belonging to Depositional Sequence B.

4.4.3. Selecting the best-fit simulation for the T unit (dep. Seq. B)

The main geometric and architectural constraints for the T unit are summarized in Fig. 7C and in the previous section 4.3. Thus, from the previous comparison and although a backstepping of platform top carbonates is recorded roughly for the lower part of the T unit in all simulations, greater amounts of terrigenous supply outputs better facies distributions (as stated in the first attempt), because: (1) only simulations with 2.0 gr/s and 2.5 gr/s show the FA I passing basinwards and upwards to basin marls (FA III), which (2) in turn overlie and mark the drowning of the underlying lowstand platform, and (3) the thickness of the FA III increases as the rate of inflowing terrigenous sediment increases (Fig. 14B) reaching 40–50 m with greater values (2.5 gr/s).

Only simulations with a rate of terrigenous supply set at 2.5 gr/s were considered to look for the best-simulation between the models considering different RSL curves (Fig. 14A). From these simulations only two scenarios (marked with **) output acceptable results although none of them matches completely the field observations. Both scenarios show a lower T unit where (1) basinal marls (FA III) passes upwards to slope-platform carbonates (FA I and II), (2) the marls bury the lowstand carbonate platform unit, and (3) the T unit overlies the HNR platform top carbonates of Depositional Sequence A. One of the two scenarios generated a thickness of FA III below the expected one (<40 m), and in the other simulation the slope deposits (FA II) are almost negligible. For this reason, a new simulation was tested setting a RSL curve between the two later simulations, defining the change in the rate of RSL rise at 20 m (600 ky) instead of 10 or 30 m.

The results of this intermediate scenario are summarized in Fig. 14C and were obtained with a RSL curve starting at −55 m (400 ky), changing the rate of RSL rise at 20 m (600 ky) and ending at 60 m (900 ky), combined with a rate of terrigenous supply set at 2.5 gr/s. With these improvements, the lower part of the T unit (between 400 and 600 ky) matches the expected geometric and facies architecture constraints and can be accepted as the best-fit simulation. In this regard, the prograding lowstand platform of Depositional Sequence B that thins towards the SE, starts to backstep and to onlap the SB that marks the top of Depositional Sequence A resulting in a NNW migration direction of the carbonate system (see white arrow in the oblique view of Fig. 14C2, platform carbonate 1). In the 2D cross-sections, it can also be noticed an apparent final progradation at the upper part of the interval simulated (black circle and white numbers 1 and 2 in Fig. 14C) just below 600 ky. As can be observed in the 3D oblique view (Fig. 14C2), this apparent progradation is an artefact due to the 2D view, and in fact corresponds to retrograding platform top carbonates (FA I) resulting from the superposition of two different carbonate platforms developed during the late T stage (marked with 1 and 2 in Fig. 14C). The first and older carbonate platform (marked with 1 in Fig. 14C) flourishes during the LNR stage and backsteps during the T stage (see cross-section Y in Fig. 14C). The second and younger carbonate platform (marked with 2 in Fig. 14C) initially develops as an isolated platform in the eastern part of the area modelled, near cross-section X. As simulation progresses, this second platform also backsteps in N and NW direction increasing its extension upwards, finally connecting with the first carbonate platform (Fig. 14C2).

On the other hand, and considering the same controlling parameters, the results obtained for the upper part of the T unit (above 600 ky) are unsatisfactory. For this unit, although an initial progradation is recorded, an apparent final retrogradation is recorded instead of the extrapolated and expected HNR unit. But, in fact, this apparent shift from progradation to retrogradation is only a change in the real migration direction in 3D that is changing from a N–S to a mainly E-W trend. This fact can be noticed in Fig. 14C1 where a W-E and N–S cross-sections are included and an apparent upper westwards progradation is recorded in the W-E cross-section while in the N–S cross-section the carbonate platform is retrograding. This suggests that the change in the stacking pattern noticed in Fig. 14B can also be related to a change in the progradation direction from N–S to E-W instead of a real retrogradation. This change may be the result of: (i) a reduction of the available accommodation, (ii) a relative constant bathymetry that in this upper T unit is more horizontal, (iii) an increase of the rate of inflowing terrigenous sediments, and (iv) a basinwards accumulation of sediment.

Given that the terrigenous supply and/or rate of RSL rise mainly constrain the stacking pattern obtained, the upper T unit will be tested again with different rates of inflowing terrigenous and RSL curves. In relation to a qualitative sensitivity analysis for this genetic type of deposit, it can be noticed a similar relationship between the development of the different facies assemblages and their controlling parameters, but, in this case, the rate of terrigenous input not only strongly controls the development of the carbonate facies assemblages but can also force to change its migration direction and the stacking pattern (note that a different stacking pattern is obtained by only increasing the rate of inflowing terrigenous sediments from 1.0 to 2.5 gr/s; Fig. 14B).

4.5. Depositional sequence B. HNR unit (2 nd attempt)

As concluded in the last section, the HNR unit of Depositional Sequence B needs to be simulated again taking into account a change in the rate of inflowing terrigenous sediment and/or the RSL curve. Bearing in mind that the existing field constraints for this genetic type of deposit are limited, different scenarios were tested to obtain different possible geometries and facies distributions under different conditions. Finally, the most probable scenario was chosen based on the available geological data.

The initial elevation of the RSL curve was set at 20 m (600 ky) from the previous T unit best-fit simulation as well as the obtained basin geometry. The different rates of RSL rise were obtained setting the final

elevation at 60 m but considering three different final time steps (800, 850 and 900 ky) (Fig. 15). Two rates of inflowing terrigenous sediment (1.0 and 2.5 gr/s) were also defined obtaining 6 different possible scenarios for this last genetic unit (Fig. 15).

4.5.1. HNR unit: effects of terrigenous supply and RSL curve

As stated also from previous modelled units, the RSL curve used and/or the amount of inflowing terrigenous produce: (1) a stacking pattern shift from retrogradation (with a lower rate of terrigenous input and/or higher rate of RSL rise) to progradation (with higher inflowing terrigenous and/or a lower rate of RSL rise), (2) this change occurs before when the amount of inflowing terrigenous is greater (RSL 600–850 for terrigenous supply 2.5 gr/s instead of 600–900 for 1.0 gr/s), (3) the drowning of the carbonate platform when the rate of RSL rise is high (RSL 600–800 ky) and the rate inflowing terrigenous is low (1.0 gr/s), (4) the increase of terrigenous sediment accumulation basinwards when the rate of RSL rise is low considering both rates of inflowing terrigenous (1.0 or 2.5 gr/s), (5) when prograding, the upper part of the genetic unit shows an apparent retrogradation which in fact is a shift in the progradation direction as previously described (section 4.4.3 and Fig. 14C1), and (6) the sedimentary infill reaches the expected stratigraphic thickness of 60 m when the rate of RSL rise is low.

4.5.2. Selecting the best-fit simulation for the upper HNR unit (dep. Seq. B)

As the outcropping conditions of this genetic unit are in 2D and is partly eroded, the selection of the best-fit simulation cannot be performed as in the previous units given that less field constraints are available. Nonetheless, from the existing outcrops, a geometric extrapolation and facies distribution of the carbonate unit is proposed (see Fig. 7C) and was used as a reference to select the "best-fit" simulation. Thus, only the simulations that (i) outputs a prograding stacking pattern, and (ii) exhibits a stratigraphic thickness of around 60 m were selected

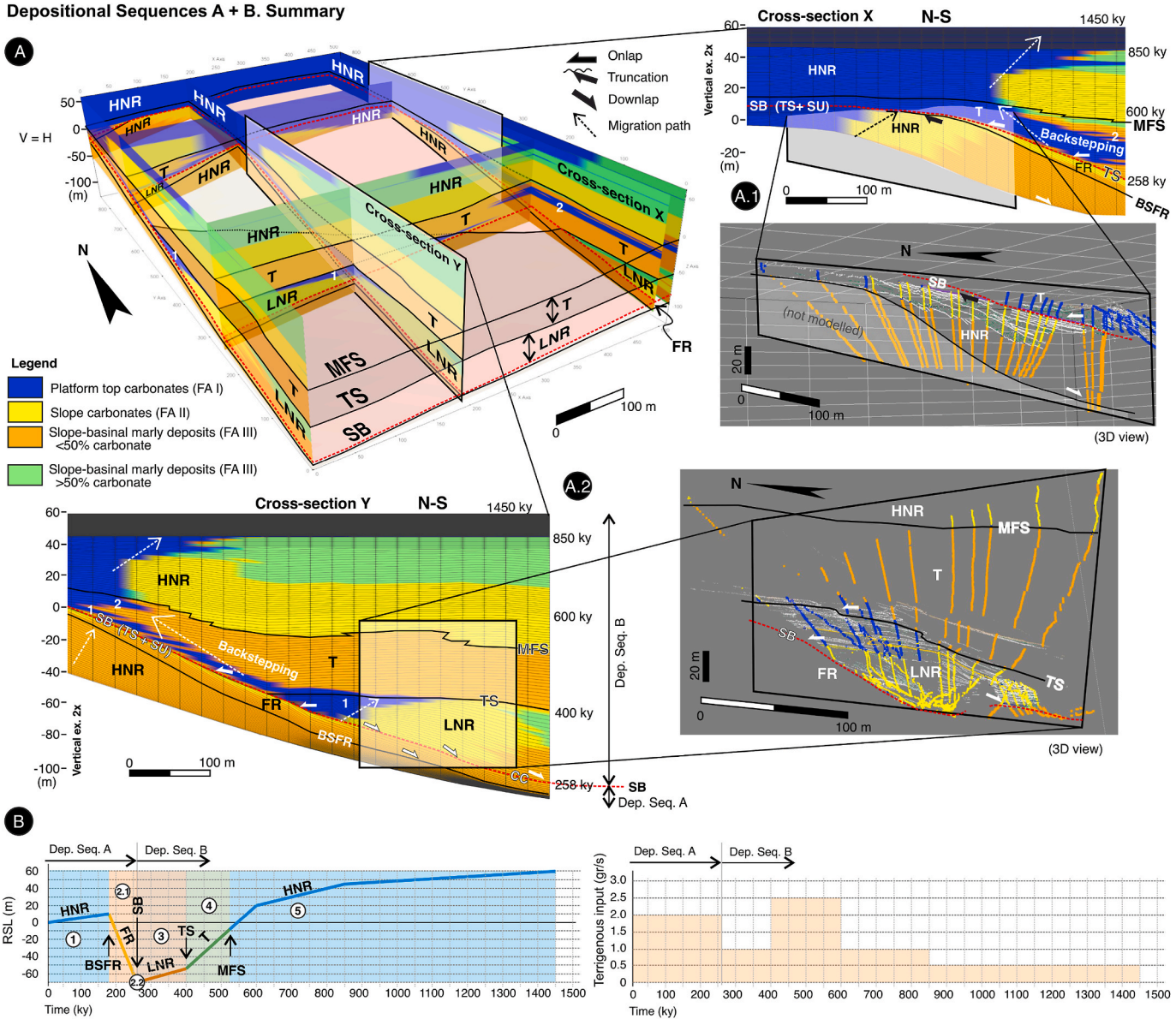

Fig. 16. Summary of the final best-fit simulation for depositional sequences A and B belonging to Las Mingachas carbonate system. A) Fence diagram displaying the facies distribution and the sequence-stratigraphic interpretation. See abbreviations in Fig. 4. Two close-up views (A.1 and A.2) for the cross-sections X and Y have been also included (note the vertical exaggeration 2x). Time lines allow identifying the stacking patterns of the distinct sedimentary bodies generated. Parts of both views are compared with the facies identified in the field through the DOM (see enlarged images). B) Rates versus time of RSL changes and terrigenous input used to obtain the final model.

(marked with ** in Fig. 15A). From the selected simulations, it can be noticed that the upper apparent retrogradation in fact corresponds to a shift in the progradation direction from S to W.

Although the resulting three models are reliable, a shift in the rate of RSL rise in the upper part of the HNR stage can be tested in order to force the system to prograde towards the S or SW instead of the W. As can be observed in Fig. 15B, defining a shift at 45 m (850 ky) of the rate of RSL rise and a rate of inflowing terrigenous of 1.0 gr/s (at 600 ky) and 0.5 gr/s (at 850 ky), favours a major prograding distance of the platform margin towards the S or SW. Note that, under these conditions, the last time step is located at 1450 ky instead of 900 ky in order to fill the available accommodation (until 60 m).

In this last modelled genetic type of deposit, and related to the qualitative sensitive analysis, it can be highlighted that, not only the slope carbonates (FA II) remain the most sensitive carbonate deposits due to the presence of terrigenous sediments, but also the stacking pattern of the platform top carbonates (FA I) show a high dependency on the input of terrigenous sediments. For instance, favouring the progradation (inflowing siliciclastic rate = 2.5 gr/s) instead of aggradation (1.0 gr/s) (Fig. 15A, RSL 600–850 ky) by increasing the substrate and the optimum water depth for this carbonate-producing association, or avoiding platform drowning (Fig. 15A, RSL 600–800 ky, for both rates of terrigenous supply).

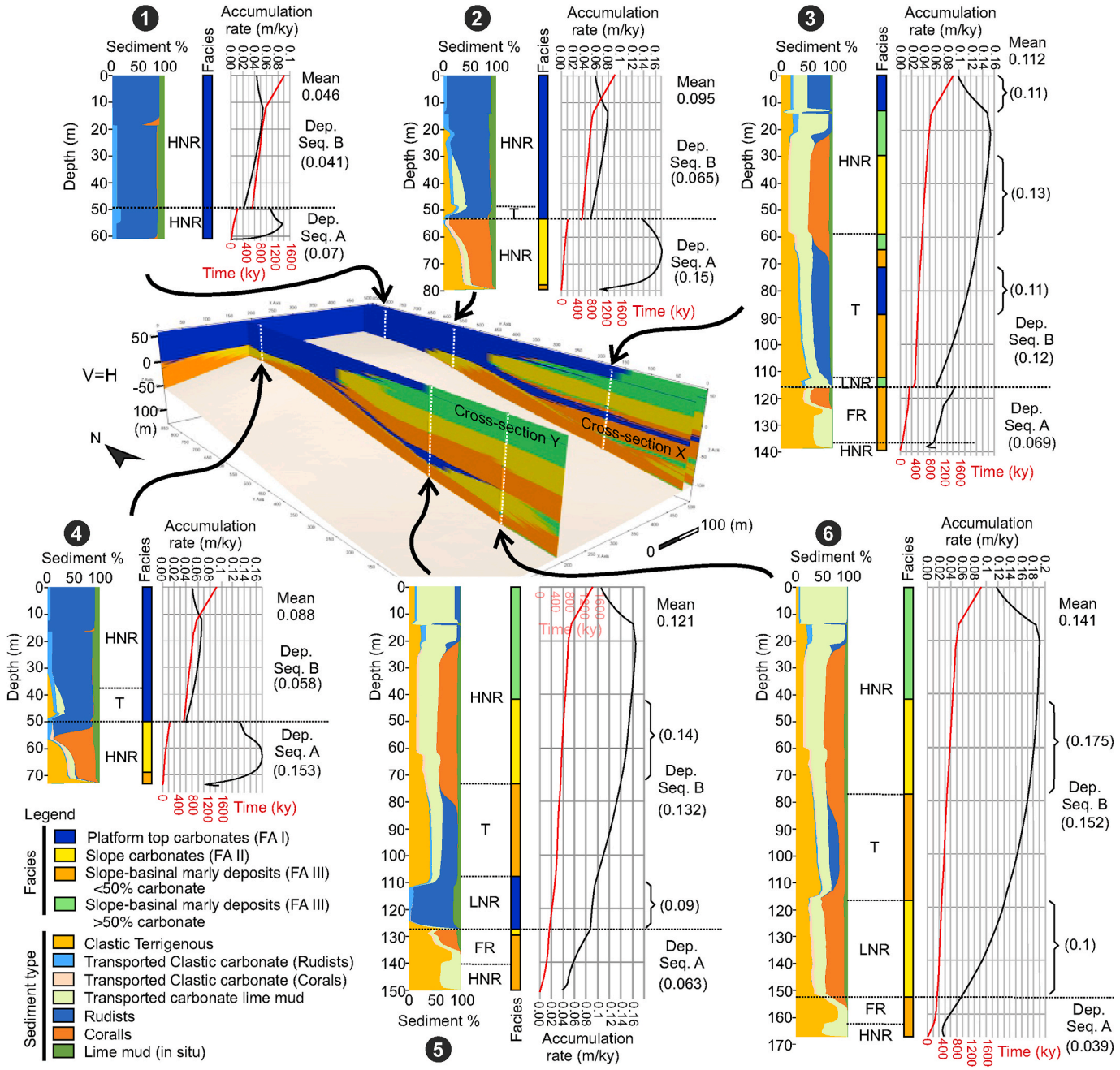

Fig. 17. Accumulation rates (m/ky, black line) obtained in the final best-fit model for selected stratigraphic well logs in which the accumulated sediment percentage and the corresponding facies are also represented. Stratigraphic well logs are located following the main cross-sections X and Y (see 3D view). The accumulation rate mean values for the total well log, for depositional sequences A and B, and for each carbonate deposit are included as well. Note the hiatus recorded in the stratigraphic well logs 1, 2, 3 and 4 due to the RSL drop between depositional sequences A and B.

5. Discussion

Taking into account the previous selected models for each genetic type of deposit, the final best-fit simulation is summarized in Fig. 16. The upper part of Depositional Sequence A was modelled setting a RSL rise from 0 to 10 m during 175 ky followed by a fast RSL fall down to −70 m at 258 ky, with an autochthonous maximum carbonate production rate set at 0.08 m/ky and an inflowing rate of terrigenous siliciclastics of 2.0 gr/s. Under these conditions, an initial HNR strata is recorded (unit 1) showing FA I, II and III stacked in a prograding pattern and displaying downlapping stratal terminations. During the falling stage, the FR strata (unit 2.1) is constituted by FA II passing basinwards to FA III and displays a progradational and downstepping clinoforms over the BSFR. Both modelled genetic units show stratal geometries, stacking patterns and a facies architecture similar to those observed in the field (Fig. 16A1; see Bover-Arnal et al., 2009, 2011). Erosion was not modelled during FR and thus no truncations are simulated in the model. However, the field-based model includes a truncation surface at the top of the HNR platform carbonates resulting from subaerial exposure during falling RSL (Fig. 16A1; Bover-Arnal et al., 2009, 2010, 2011). Nevertheless, this fall in RSL and related truncation of platform top highstand strata is inferred from the sedimentary hiatus obtained at the boundary between depositional sequences A and B in proximal settings of the carbonate system modelled (see Fig. 17, stratigraphic logs 1, 2, 3 and 4).

The late early Aptian basin floor wedge (Figs. 10 and 11) interpreted as a forced regression by Bover-Arnal et al. (2009) (Fig. 4) was later re-interpreted as a transgressive unit by Peropadre et al. (2013), Pomar and Haq (2016) and Pomar (2020). The present publication is not focused on interpreting again available field evidence that indicates regression during the deposition of this basin floor component or on discussing alternative interpretations. However, a major sea-level drop with an amplitude between 60 and 70 m occurred during the late early Aptian in this western sub-basin of the Maestrat Basin. This drop in sea level is evidenced by the presence of late early Aptian incised valleys with maximum depths of 60–70 m carved on highstand platform top carbonates of the Villarroya de los Pinares Formation (Peropadre et al., 2007; Bover-Arnal et al., 2009, 2010, 2011, 2016). In the modelled platform margin, the height difference between the late early Aptian forced regressive wedge and the preserved highstand platform top, which is located topographically above (Figs. 4 and 7), is about 64 m (Bover-Arnal et al., 2009). Thus, this height difference, which is indicative of the magnitude of the late early Aptian RSL drop at the platform-to-basin transition area modelled, is in accordance with the amplitude of RSL drop recorded as incised valleys in inner platform settings.

The presented 3D numerical model shows that during the simulated late early Aptian base-level fall sedimentation of FAII occurred topographically below and basinwards of a HNR platform, and above basinal deposits of FAIII (Figs. 1, 7, 10 and 116-17). This FR unit made up of reworked and resedimented shallow water components accumulated as a basin floor wedge, while landwards a highstand platform top constituted by FAI was subaerially exposed (Figs. 7 and 16). Therefore, the combination of controlling parameters set to obtain the best-fit depositional architecture and the simulation achieved (Figs. 1, 7, 10 and 116-17) result in a sedimentary evolution similar to that described by Bover-Arnal et al. (2009). Overall, these model results challenge the transgressive nature of this basin floor component proposed by Peropadre et al. (2013), Pomar and Haq (2016) and Pomar (2020).

The LNR unit of Depositional Sequence B deposited during the stillstand and the subsequent base-level rise was simulated from −70 m to −55 m (258 and 400 ky, respectively) (unit 3). If autochthonous maximum carbonate production rate remains similar (0.08 m/ky) to that from the previous stages, the inflowing terrigenous siliciclastic sediment needs to be reduced to 1.0 gr/s allowing the development of the FA I passing basinwards to FA II and III. Note that the relatively small carbonate platform stacked in a prograding-aggrading pattern is developed predominantly along the western side of the modelled area, parallel to the shoreline and thins in a NW-SE direction (see number 1 in Fig. 16A). The deposits formed show onlapping clinoforms towards the land and onto the SU while slope carbonates downlap onto the CC (Fig. 16A2).

By defining a shift on the rate of RSL rise at 400 ky (setting the RSL elevation to 20 m at 600 ky), the previous LNR evolves to a T genetic type of deposit (unit 4), and the prograding lowstand carbonate platform (number 1, Fig. 16A) starts to backstep until it drowns. As the carbonate platform top facies passes upwards and basinwards to basinal marls (FA III) and no FA II occurs, the rate of terrigenous supply needs to be increased to, at least, 2.5 gr/s. As transgression progresses, a second carbonate platform developed at the SE part of the modelled area, which does not crop out in the field (number 2, Fig. 16A–A1). This second carbonate platform is also stacked in a retrograding pattern but in this case, due to an increase of its extension updip, both backstepping carbonate platforms connect northwestwards (see Fig. 14C2).

Prior to reaching the highest RSL elevation during this rising stage (20 m at 600 ky), the simulation shows the occurrence of the FA II on top of thick basinal-marly deposits (550 ky) allowing the identification of the MFS marking the top of the T unit (below) from the subsequent HNR above (unit 5). During this last HNR stage, a large and extensive aggrading carbonate platform developed with FA I evolving basinwards into FA II.

From 600 ky on, the RSL decreases both its rising rate and the inflowing siliciclastic sediment rate until it reaches the last and highest RSL elevation modelled (60 m at 1450 ky). In this respect, to record a final prograding stacking pattern and to favour the growth of the most extensive carbonate platform developed in the studied carbonate system (although currently partly eroded), the RSL elevation should be set to 45 m (850 ky) and the rate of inflowing terrigenous must be decreased from 2.5, to 1.0 and finally to 0.5 gr/s.

The final simulated RSL curve (Fig. 16B) is realistic and was set taking into account the amplitudes and timing of the eustatic late early-early late Aptian sea-level changes reported from the Maestrat Basin but also recorded along the margin of the Tethys. In the Maestrat Basin, a late early Aptian sea-level highstand and a subsequent fall in sea level of around 60–70 m occurred (Peropadre et al., 2007; Bover-Arnal et al., 2009, 2010, 2011, 2016). This sea-level drop was followed by a latest early-early late Aptian base-level rise of similar magnitude (Fig. 16B; Bover-Arnal et al., 2009, 2010, 2016). The succession modelled contains ammonites belonging to the *Dufrenoyia furcata* and *Epicheloniceras martini* ammonite zones (Fig. 7; Bover-Arnal et al., 2009, 2010, 2016; Moreno-Bedmar et al., 2010; Garcia et al., 2014) and thus, according to the numerical ages of Gradstein et al. (2004) would have been deposited in less than 2 My (Figs. 3 and 16B).

In other basins of the Tethys, this late early Aptian major fall in sea level, and subsequent base-level rise, also recorded amplitudes comparable to those measured in the Maestrat Basin and thus set for the simulated RSL curve (Fig. 16B). For example, incised valleys of around 50 m deep were developed during the late early Aptian on platform carbonates facing the Vocontian Basin (Arnaud-Vanneau and Arnaud, 1990; Hunt and Tucker, 1993). In a review of Cretaceous sea-level fluctuations, Ray et al. (2019) give amplitudes of sea-level change of up to 60 m with sporadic larger events for the Aptian. The late early-early late Aptian Shu'aiba Formation in the Middle East was also subaerially exposed as a result of a major sea-level fall of tens-of-metres (e.g., Hillgärtner et al., 2003; van Buchem et al., 2010; Yose et al., 2010). In this regard, the sea-level lowering in the Arabian Plate subaerially exposed and incised a highstand platform and favoured the basinwards development of a topographically lower prograding lowstand platform (Yose et al., 2006, 2010; Maurer et al., 2010, 2013; Pierson et al., 2010). Thus, the resulting depositional and facies architecture of this coeval carbonate system from the Arabian Plate shows strong similarities to the one modelled from the western Maestrat Basin (Figs. 4, 7 and 16).

From the final best-fit simulation, the apparent accumulation rate (in m/ky) can be analysed through different stratigraphic logs in the different depositional settings within the platform-to-basin transition area modelled (Fig. 17). In this sense, the mean accumulation rate shows the lower values near the platform area (0.046 and 0.088 m/ky, stratigraphic logs 1 and 4, respectively) and higher values basinwards (0.112 and 0.141 m/ky, stratigraphic logs 3 and 6, respectively) as accommodation increases. Specifically, for the platform carbonate deposits of FA I, the accumulation rate also increases basinwards (for example in cross-section X, Fig. 17, ranging from 0.046 to 0.11 m/ky at stratigraphic logs 1 and 3, respectively) and shows a lesser mean value of 0.079 m/ky in comparison with the mean values obtained for the slope carbonate deposits of FA II (0.14 m/ky), although both facies assemblages were set with the same maximum autochthonous carbonate production rate. This difference results from the distinct accommodation available (due to the different water depths for maximum carbonate production) and the major contribution of the siliciclastic sediments on the slope facies.

Although compaction processes were not modelled due to the lack of information, the simulated maximum autochthonous carbonate production of 0.08 m/ky, and the corresponding final accumulation rates varying from 0.046 to 0.141 m/ky, are in accordance with those proposed by Reading (1996) for Cretaceous ancient carbonates (ranging between 0.05 and 0.18 m/ky). The carbonate production and accumulation values obtained also match the low-production carbonate model suggested by Pohl et al. (2019) for coral- and rudist-bearing low-latitude (~30° NS) Aptian carbonate systems.

6. Conclusions

The effect of three main controlling parameters (carbonate production rate, RSL changes, and siliciclastic input) through time on facies distribution and stratigraphic architecture has been tested on an Aptian carbonate system using forward numerical modelling. By setting a range of possible values for each variable and their combination, 522 numerical simulations or possible 3D geological scenarios have been obtained by means of the SIMSAFADIM-CLASTIC code.

From the relative limited field data (seismic or well data do not exist in this area) combined with a virtual 3D digital outcrop model (DOM), a range of qualitative (architecture and stacking patterns) and/or quantitative (geometric) constraints have been used to perform the best-fit simulation selection from the obtained scenarios. This selection process has been conducted sequentially for each genetic type of deposit (systems tract), reducing the number of simulations and constraining, if possible, the controlling parameters values for the subsequent stage. Although the combination of these values results in a wide range of possible scenarios, finally only few simulations match the qualitative and quantitative constraints based on field observations. If new data is gathered from the field or by means of indirect methods, new simulations could be performed to (i) fine-tune the simulation selection or the related best-fit controlling parameters, and (ii) to reduce uncertainties.

Determining the effect of each controlling parameter alone is difficult to construe given that the final sedimentary deposit always results from the interplay between several variables. In the modelling performed herein, the relative weight of each variable has been addressed by comparing those simulations in which two controlling parameters remain equal while the third one changes. In this regard, the fluctuation of RSL combined with the existing bathymetry has proven to be the main environmental parameter controlling the generation of the accommodation, and thus sets the position and initial development of carbonate deposits. However, once the position of the carbonate factory is settled, the resulting geometry, dimensions and stacking patterns of the carbonate bodies generated can be also influenced and controlled by the rates of inflowing terrigenous sediment and autochthonous carbonate production. Furthermore, the importance of each controlling factor can change in function of the carbonate producing organisms considered.

The different simulations performed indicate that the platform top facies (FA I) is the most sensitive assemblage to RSL change and thus to its rising or falling ratios. FA I shows a moderate sensitivity to terrigenous input and changes in the carbonate production rate. The inflowing terrigenous sediment influences both, the carbonate platform extension but also the stacking pattern obtained. For instance, when sediment settles it can (1) avoid the platform drowning by keeping an optimum water depth for the carbonate-producing organisms, (2) increase the available substrate basinwards for a fast extension (and progradation) of the platform, or (3) force a change in the progradation direction.

In contrast, although the position of the slope deposits (FA II) is also determined by the elevation of the base level, this FA shows to be more sensitive to the presence of siliciclastic sediment than to changes of RSL, and moderately to the variations in the autochthonous carbonate production rate. Thus, when the terrigenous input is relatively high or the carbonate production rate is relatively low, the slope facies assemblage develops in restricted and narrower belts, or even disappears.

Quantitatively the final numerical model sets a RSL elevation shifting from 0, 10, −70, −55, 20, 45 and 60 m at 0, 175, 258, 400, 600, 850 and 1450 ky, respectively. Under these conditions, simulation outputs five different genetic types of deposit belonging to two depositional sequences as expected. The main features and key parameters for each genetic unit have been simulated by the code reducing the initial uncertainties and quantifying the main controlling parameters. The best-fit simulations run were set with an inflowing clastic terrigenous sediment rate ranging between 0.5 and 2.5 gr/s and a maximum autochthonous carbonate production rate of 0.08 m/ky resulting in a mean accumulation rate of 0.079 and 0.14 m/ky for the FA I and II, respectively. These production and accumulation ratios obtained fall within the expected range reported from the literature for Cretaceous carbonate deposits.

The 3D simulation obtained depicts the geometry, distribution and relationships between the different carbonate deposits generated increasing the understanding of subsurface carbonate reservoirs clearly below the seismic scale and generated in platform-to-basin depositional systems sequentially controlled by highstand normal regressive, forced regressive, lowstand normal regressive and transgressive stages of relative sea level. For instance, the resulting 3D model allows to identify two different and initially disconnected carbonate platforms developed during the LNR stage not identified in the field. These platforms are later connected during the subsequent T of RSL evolving into a large and extensive flat-topped non-rimmed platform. Thus, results also have important implications for: (1) predicting lithofacies distribution, (2) testing reservoir connectivity in subsurface carbonate reservoirs, (3) quantifying reservoir dimensions and volumes, and (4) avoiding erroneous interpretations of apparent relationships between sedimentary bodies from the analysis of 2D data (e.g., seismic, cross-sections or field outcrops).

Credit author statement

Òscar Gratacós: Methodology, Writing – original draft, Conceptualization, Software, Validation, Formal analysis, Investigation, Writing – review & editing, Visualization, Project administration **Telm Bover-Arnal**: Conceptualization, Writing – original draft, Validation, Investigation **Roger Clavera-Gispert**: Methodology, Software, Resources **Ana Carmona**: Methodology, Software, Resources **David García-Sellés**: Methodology, Software, Resources

Declaration of competing interest

The authors declare that they have no known competing financial interests or personal relationships that could have appeared to influence the work reported in this paper.

Acknowledgements

This research was carried out in the Geomodels Research Institute at

the Universitat de Barcelona. Funding for this study came from the I + D + i research project CGL2015-60805-P (BIOGEOEVENTS) (MINECO, FEDER, EU), CGL-2017-85532-P (SALCONBELT) (MINECO, FEDER, EU), the Grup de Recerca Reconegut per la Generalitat de Catalunya 2017 SGR 824 "Geologia Sedimentària", and the Geodynamics and Basin Analysis Group (GGAC) as a Grup de Recerca Consolidat per la Generalitat de Catalunya 2017SGR596. Petex and Paradigm[MT] are thanked for providing academic licenses for Move and GoCad softwares, respectively, used in the 3D reconstruction and restoration processes. We are grateful to John J.G. Reijmer and to an anonymous reviewer for their insightful and detailed comments that helped to improve the manuscript.

References

Abreu, V., 1998. Evolution of the Conjugate Volcanic Passive Margins: Pelotas Basin (Brazil) and Offshore Namibia (Africa): Implication for Global Sea-Level Changes. Unpublished Ph.D. thesis. Rice University, Houston, p. 355.

Arnaud-Vanneau, A., Arnaud, H., 1990. Hauterivian to Lower Aptian carbonate shelf sedimentation and sequence stratigraphy in the Jura and northern subalpine chains (southeastern France and Swiss Jura). In: Tucker, M.E., Wilson, J.L., Crevello, P.O., Sarg, J.R., Read, J.F. (Eds.), Carbonate Platforms. International Association of Sedimentologists, vol. 9, pp. 203–233. Special Publications.

Bitzer, K., Salas, R., 2002. SIMSAFADIM: three-dimensional simulation of stratigraphic architecture and facies distribution modeling of carbonate sediments. Comput. Geosci. 28, 1177–1192.

Borgomano, J.R.F., Fournier, F., Viseur, S., Rijkels, L., 2008. Stratigraphic well correlations for 3-D static modeling of carbonate reservoirs. AAPG (Am. Assoc. Pet. Geol.) Bull. 92, 789–824.

Bover-Arnal, T., Salas, R., Moreno-Bedmar, J.A., Bitzer, K., 2009. Sequence stratigraphy and architecture of a late Early-Middle Aptian carbonate platform succession from the western Maestrat Basin (Iberian Chain, Spain). Sediment. Geol. 219, 280–301.

Bover-Arnal, T., Moreno-Bedmar, J.A., Salas, R., Skelton, P.W., Bitzer, K., Gili, E., 2010. Sedimentary evolution of an Aptian syn-rift carbonate system (Maestrat Basin, E Spain): effects of accommodation and environmental change. Geol. Acta 8, 249–280.

Bover-Arnal, T., Salas, R., 2010. Outcrops with seismic-scale geometries: an aptian example from the western Maestrat Basin (E Iberia). In: 72nd EAGE Conference & Exhibition Incorporating SPE EUROPEC 2010, Barcelona, Spain, pp. 14–17. June 2010. Abstracts, J015.

Bover-Arnal, T., Salas, R., Skelton, P.W., Gili, E., Moreno-Bedmar, J.A., 2011. The Aptian carbonate platforms of the western Maestrat Basin: a textbook example of four systems tract-based sequence stratigraphy. In: Arenas, C., Pomar, L., Colombo, F. (Eds.), Pre-Meeting Field trips Guidebook, 28th IAS Meeting, Zaragoza. Sociedad Geológica de España, Geo-Guías, vol. 7, pp. 27–64.

Bover-Arnal, T., Löser, H., Moreno-Bedmar, J.A., Salas, R., Strasser, A., 2012. Corals on the slope (aptian, Maestrat Basin, Spain). Cretac. Res. 37, 43–64.

Bover-Arnal, T., Pascual-Cebrian, E., Skelton, P.W., Gili, E., Salas, R., 2015. Patterns in the distribution of Aptian rudists and corals within a sequence-stratigraphic framework (Maestrat Basin, E Spain). Sediment. Geol. 321, 86–104.

Bover-Arnal, T., Moreno-Bedmar, J.A., Frijia, G., Pascual-Cebrian, E., Salas, R., 2016. Chronostratigraphy of the barremian-early albian of the Maestrat Basin (E iberian Peninsula): integrating strontium-isotope stratigraphy and ammonoid biostratigraphy. Newsl. Stratigr. 49, 41–68.

Canérot, J., Cugny, P., Pardo, G., Salas, R., Villena, J., 1982. Ibérica central-maestrazgo. In: García, A. (Ed.), El Cretácico de España. Universidad Complutense de Madrid, pp. 273–344.

Carmona, A., 2016. Combining Discrete Element and Process-Based Sedimentary Models: a New Tool to Model Syntectonic Sedimentation. PhD Thesis. Universitat de Barcelona, p. 157. http://hdl.handle.net/2445/108806.

Carmona, A., Clavera-Gispert, R., Gratacós, O., Hardy, S., 2010. Modelling syntectonic sedimentation: combining a discrete element model of tectonic deformation and a process-based sedimentary model in 3d. Math. Geosci. 42 (5), 519–534. https://doi.org/10.1007/s11004-010-9293-6.

Carmona, A., Gratacós, O., Clavera-Gispert, R., Muñoz, J.A., Hardy, S., 2016. Numerical modelling of syntectonic subaqueous sedimentation: the effect of normal faulting and a relay ramp on sediment dispersal. Tectonophysics 684, 100–118.

Catuneanu, O., Abreu, V., Bhattacharya, J.P., Blum, M.D., Dalrymple, R.W., Eriksson, P. G., Fielding, C.R., Fisher, W.L., Galloway, W.E., Gibling, M.R., Giles, K.A., Holbrook, J.M., Jordan, R., Kendall, C.G.StC., Macurda, B., Martinsen, O.J., Miall, A. D., Neal, J.E., Nummedal, D., Pomar, L., Posamentier, H.W., Pratt, B.R., Sarg, J.F., Shanley, K.W., Steel, R.J., Strasser, A., Tucker, M.E., Winker, C., 2009. Towards the standardization of sequence stratigraphy. Earth Sci. Rev. 92, 1–33.

Catuneanu, O., 2020. Sequence stratigraphy in the context of the 'modeling revolution'. Mar. Petrol. Geol. 116 (104309) https://doi.org/10.1016/j.marpetgeo.2020.104309.

Clavera-Gispert, R., Carmona, A., Gratacós, O., Tolosana-Delgado, R., 2012. Incorporating nutrients as a limiting factor in carbonate modelling. Palaeogeogr. Palaeoclimatol. Palaeoecol. 329–330, 150–157. https://doi.org/10.1016/j.palaeo.2012.02.025.

Clavera-Gispert, R., 2016. Forward Numerical Modelling of Carbonate Basins: an Ecological Approach. PhD Thesis. Technische Universität Bergakademie Freiberg, Freiberg, Germany, p. 152.

Clavera-Gispert, R., Gratacós, O., Carmona, A., Tolosana-Delgado, R., 2017. Process-based forward numerical ecological modeling for carbonate sedimentary basins. Comput. Geosci. 21, 373–391. https://doi.org/10.1007/s10596-017-9617-4.

Debenay, J.P., André, J.P., Lesourd, M., 1999. Production of lime mud by breakdown of foraminiferal tests. Mar. Geol. 157 (3–4), 159–170. https://doi.org/10.1016/S0025-3227(98)00151-0.

Embry, J.-C., Vennin, E., van Buchem, F.S.P., Schroeder, R., Pierre, C., Aurell, M., 2010. Sequence stratigraphy and carbon isotope stratigraphy of an Aptian mixed carbonate-siliciclastic platform to basin transition (Galve sub-basin, NE Spain). In: van Buchem, F.S.P., Gerdes, K.D., Esteban, M. (Eds.), Mesozoic and Cenozoic Carbonate Systems of the Mediterranean and the Middle East: Stratigraphic and Diagenetic Reference Models, vol. 329. Geological Society Special Publications, London, pp. 113–143.

Ferguson, R.I., Church, M.A., 2004. A simple universal equation for grain settling velocity. J. Sediment. Res. 74, 933–937.

Fernández-Mendiola, P.A., Mendicoa, J., Hernandez, S., Owen, H.G., García-Mondéjar, J., 2013. A facies model for an Early Aptian carbonate platform (Zamaia, Spain). Facies 59, 529–558.

Finch, E., Hardy, S., Gawthorpe, R., 2003. Discrete element modelling of contractional faults-propagation folding above rigid basement rocks. J. Struct. Geol. 25, 515–528.

Finch, E., Hardy, S., Gawthorpe, R., 2004. Discrete element modelling of extensional faults-propagation folding above rigid basement rocks. Basin Res. 16, 489–506.

Garcia, R., Moreno-Bedmar, J.A., Bover-Arnal, T., Company, M., Salas, R., Latil, J.L., Martín-Martín, J.D., Gomez-Rivas, E., Bulot, L.G., Delanoy, G., Martínez, R., Grauges, A., 2014. Lower cretaceous (Hauterivian-Albian) ammonite biostratigraphy in the Maestrat Basin (E Spain). J. Iber. Geol. 40, 99–112.

Geyer, A., García-Sellés, D., Pedrazzi, D., Barde-Cabusson, S., Martí, J., Muñoz, J.A., 2015. Studying monogenetic volcanoes with a terrestrial laser scanner: case study at Croscat volcano (Garrotxa Volcanic Field, Spain). Bull. Volcanol. 77 (3), 1–14. https://doi.org/10.1007/s00445-015-0909-z.

Gili, E., Skelton, P.W., Bover-Arnal, T., Salas, R., Obrador, A., Fenerci-Masse, M., 2016. Depositional biofacies model for post-OAE1a aptian carbonate platforms of the western Maestrat Basin (iberian Chain, Spain). Palaeogeogr. Palaeoclimatol. Palaeoecol. 453, 101–114.

Gili, E., Götz, S., 2018. Part N, volume 2, chapter 26B: paleoecology of rudists. Treatise Online 103, 1–29, 22 fig.

Griffiths, C.M., 1996. Computer modelling of basin fill. In: Emery, D., Myers, K. (Eds.), Sequence Stratigraphy. Blackwell Science Ltd, London, pp. 258–269.

Gradstein, F.M., Ogg, J.G., Smith, A.G. (Eds.), 2004. A Geologic Time Scale 2004. Cambridge University Press, Cambridge, p. 589.

Gratacós, O., 2004. SIMSAFADIM-CLASTIC: Modelización 3D de transporte y sedimentación clástica subacuática (3D modelling of clastic transport and deposition). Ph.D. thesis. Universitat de Barcelona, p. 256.

Gratacós, O., Bitzer, K., Cabrera, L., Roca, E., 2009a. SIMSAFADIM-CLASTIC: a new approach to mathematical 3D forward simulation modelling for clastic and carbonate sedimentation. Geol. Acta 7, 311–322.

Gratacós, O., Bitzer, K., Casamor, J.L., Cabrera, L., Calafat, A., Canals, M., Roca, E., 2009b. Simulating transport and deposition of clastic sediments in an elongate basin using the SIMSAFADIM-CLASTIC program: the Camarasa artificial lake case study (NE Spain). Sediment. Geol. 222 (1–2), 16–26. https://doi.org/10.1016/j.sedgeo.2009.05.010.

Hardy, S., Finch, E., 2005. Discrete-element modelling of detachment folding. Basin Res. 17, 507–520.

Hillgärtner, H., Van Buchem, F.S.P., Gaumet, F., Razin, P., Pittet, B., Grötsch, J., Droste, H., 2003. The Barremian-Aptian evolution of the eastern Arabian carbonate platform margin (northern Oman). J. Sediment. Res. 73, 756–773.

Hunt, D., Tucker, M.E., 1992. Stranded parasequences and the forced regressive wedge systems tract: deposition during base-level fall. Sediment. Geol. 81, 1–29.

Hunt, D., Tucker, M.E., 1993. Sequence stratigraphy of carbonate shelves with an example from the mid-Cretaceous (Urgonian) of southeast France. In: Posamentier, H.W., Summerhayes, C.P., Haq, B.U., Allen, G.P. (Eds.), Sequence Stratigraphy and Facies Associations. International Association of Sedimentologists, vol. 18. Special Publications, pp. 307–341.

Hunt, D., Tucker, M.E., 1995. Stranded parasequences and the forced regressive wedge systems tract: deposition during base-level fall—reply. Sediment. Geol. 95, 147–160.

James, N.P., Bone, Y., 1991. Origin of a cool-water, Oligo-Miocene deep shelf limestone, Eucla Platform, southern Australia. Sedimentology 38, 323–341.

Martín-Chivelet, J., López-Gómez, J., Aguado, R., Arias, C., Arribas, J., Arribas, M.E., Aurell, M., Bádenas, B., Benito, M.I., Bover-Arnal, T., Casas-Sáinz, A., Castro, J.M., Coruña, F., de Gea, G.A., Fornós, J.J., Fregenal-Martínez, M., García-Senz, J., Garófano, D., Gelabert, B., Giménez, J., González-Acebrón, J., Guimerà, J., Liesa, C. L., Mas, R., Meléndez, N., Molina, J.M., Muñoz, J.A., Navarrete, R., Nebot, M., Nieto, L.M., Omodeo-Salé, S., Pedrera, A., Peropadre, C., Quijada, I.E., Quijano, M.L., Reolid, M., Robador, A., Rodríguez-López, J.P., Rodríguez-Perea, A., Rosales, I., Ruiz-Ortiz, P.A., Sàbat, F., Salas, R., Soria, A.R., Suarez-Gonzalez, P., Vilas, L., 2019. The late jurassic-early cretaceous rifting. In: Quesada, C., Oliveira, J.T. (Eds.), The Geology of Iberia: A Geodynamic Approach. Volume 5: the Alpine Cycle. Springer, Heidelberg, pp. 60–63. https://doi.org/10.1007/978-3-030-11295-0_5.

Maurer, F., Al-Mehsin, K., Pierson, B.J., Eberli, G.P., Warrlich, G., Drysdale, D., Droste, H.J., 2010. Facies characteristics and architecture of upper aptian Shu'aiba clinoforms in abu dhabi. In: van Buchem, F.S.P., Al-Husseini, M.I., Maurer, F., Droste, H.J. (Eds.), Barremian – Aptian Stratigraphy and Hydrocarbon Habitat of the Eastern Arabian Plate. GeoArabia Special Publication 4, vol. 2. Gulf PetroLink, Bahrain, pp. 445–468.

Maurer, F., van Buchem, F.S.P., Eberli, G.P., Pierson, B.J., Raven, M.J., Larsen, P.-H., Al-Husseini, M.I., Vincent, B., 2013. Late Aptian long-lived glacio-eustatic lowstand recorded on the Arabian Plate. Terra. Nova 25, 87–94.

Moreno-Bedmar, J.A., Company, M., Bover-Arnal, T., Salas, R., Delanoy, G., Martínez, R., Grauges, A., 2009. Biostratigraphic characterization by means of ammonoids of the lower aptian oceanic anoxic event (OAE1a) in the eastern iberian Chain (Maestrat Basin, eastern Spain). Cretac. Res. 30, 864–872.

Moreno-Bedmar, J.A., Company, M., Bover-Arnal, T., Salas, R., Delanoy, G., Maurrasse, F.J., Grauges, A., Martínez, R., 2010. Lower aptian ammonite biostratigraphy in the Maestrat Basin (eastern iberian Chain, eastern Spain). A tethyan transgressive record enhanced by synrift subsidence. Geol. Acta 8, 281–299.

Nelsen, J.E., Ginsburg, R.N., 1986. Calcium carbonate production by epibionts on Thalassia in Florida Bay. J. Sediment. Res. 56 (5), 622–628. https://doi.org/10.1306/212F89EF-2B24-11D7-8648000102C1865D.

Neumann, A.C., Land, L.S., 1975. Lime mud deposition and calcareous algae in the Bight of Abaco, Bahamas; a budget. J. Sediment. Res. 45 (4), 763–786. https://doi.org/10.1306/212F6E3D-2B24-11D7-8648000102C1865D.

Peropadre, C., Meléndez, N., Liesa, C.L., 2007. A 60 metres Aptian sea-level fall from the Galve sub-basin (Eastern Spain). In: 25th IAS Meeting of Sedimentology, Abstract vol., Patras, Greece, September 2007, p. 27.

Peropadre, C., Liesa, C.L., Meléndez, N., 2013. High-frequency, moderate to high-amplitude sea-level oscillations during the late Early Aptian: insights into the mid-Aptian event (Galve sub-basin, Spain). Sediment. Geol. 294, 233–250.

Pierson, B.J., Eberli, G.P., Al-Mehsin, K., Al-Menhali, S., Warrlich, G., Droste, H.J., Maurer, F., Whitworth, J., Drysdale, D., 2010. Seismic stratigraphy and depositional history of the upper Shu'aiba (late aptian) in the UAE and Oman. In: van Buchem, F. S.P., Al-Husseini, M.I., Maurer, F., Droste, H.J. (Eds.), Barremian – Aptian Stratigraphy and Hydrocarbon Habitat of the Eastern Arabian Plate, vol. 2. GeoArabia Special Publication 4, Gulf PetroLink, Bahrain, pp. 411–444.

Plint, A.G., 1988. Sharp-based shoreface sequences and "offshore bars" in the Cardium Formation of Alberta; their relationship to relative changes in sea level. In: Wilgus, C.K., Hastings, B.S., Kendall, C.G.StC., Posamentier, H.W., Ross, C.A., Van Wagoner, J.C. (Eds.), Sea Level Changes — an Integrated Approach. Special Publication, 42. Society of Economic Paleontologists and Mineralogists (SEPM), pp. 357–370.

Pohl, A., Laugié, M., Borgomano, J., Michel, J., Lanteaume, C., Scotese, C.R., Frau, C., Poli, E., Donnadieu, Y., 2019. Quantifying the paleogeographic driver of Cretaceous carbonate platform development using paleoecological niche modeling. Palaeogeogr. Palaeoclimatol. Palaeoecol. 514, 222–232.

Pomar, L., Haq, B.U., 2016. Decoding depositional sequences in carbonate systems: concepts vs experience. Global Planet. Change 146, 190–225.

Pomar, L., 2020. Carbonate systems. In: Scarselli, N., Adam, J., Chiarella, D., Roberts, D. G., Bally, A.W. (Eds.), Regional Geology and Tectonics. Volume 1: Principles of Geologic Analysis. Elsevier, pp. 235–311.

Posamentier, H.W., Kolla, V., 2003. Seismic geomorphology and stratigraphy of depositional elements in deep-water settings. J. Sediment. Res. 73, 367–388.

Ray, D.C., van Buchem, F.S.P., Baines, G., Davies, A., Gréselle, B., Simmons, M.D., Robson, C., 2019. The magnitude and cause of short-term eustatic Cretaceous sea-level change: a synthesis. Earth Sci. Rev. 197, 102901.

Reading, H.G., 1996. Sedimentary Environments: Processes, Facies and Stratigraphy, third ed. Blackwell, Oxford, p. 689.

Salas, R., Casas, A., 1993. Mesozoic extensional tectonics, stratigraphy, and crustal evolution during the Alpine cycle of the eastern Iberian basin. Tectonophysics 228, 33–55.

Salas, R., Guimerà, J., Martín-Closas, C., Meléndez, A., Alonso, A., 2001. Evolution of the mesozoic central iberian rift system and its cainozoic inversion (iberian Chain). In: Ziegler, P.A., Cavazza, W., Roberston, A.H.F., Crasquin-Soleau, S. (Eds.), Peri-Tethys Memoir 6: Peri-Tethyan Rift/Wrench Basins and Passive Margins. Mémoires du Muséum National d'Histoire Naturelle, Paris, vol. 186, pp. 145–186.

Schlager, W., 1981. The paradox of drowned reefs and carbonate platforms. Bull. Geol. Soc. Am. 92, 197–211.

Skelton, P.W., Gili, E., Bover-Arnal, T., Salas, R., Moreno-Bedmar, J.A., 2010. A new species of *Polyconites* from the uppermost Lower Aptian of Iberia and the early evolution of polyconitid rudists. Turk. J. Earth Sci. 19, 557–572.

Steefel, C., MacQuarrie, K., 1996. Approaches to modeling of reactive transport in porous media. In: Lichtner, P., Steefel, C., Oelkers, E. (Eds.), Reactive Transport in Porous Media, Reviews in Mineralogy, vol. 34, pp. 85–129.

Syvitski, J.P.M., Hutton, E., 2001. 2D SEDFLUX 1.0C: an advanced process–response numerical model for the fill of marine sedimentary basins. Comput. Geosci. 27, 731–753.

van Buchem, F.S.P., Al-Husseini, M.I., Maurer, F., Droste, H.J., Yose, L.A., 2010. Sequence-stratigraphic synthesis of the Barremian – Aptian of the eastern Arabian Plate and implications for the petroleum habitat. In: van Buchem, F.S.P., Al-Husseini, M.I., Maurer, F., Droste, H.J. (Eds.), Barremian – Aptian Stratigraphy and Hydrocarbon Habitat of the Eastern Arabian Plate, vol. 1. GeoArabia Special Publication 4, Gulf PetroLink, Bahrain, pp. 9–48.

Vennin, E., Aurell, M., 2001. Stratigraphie sequentielle de l'Aptien du sous-basin de Galvé (Province de Teruel, NE de l'Espagne). Bull. Soc. Geol. Fr. 172 (4), 397–410.

Vergés, J., Poprawski, Y., Almar, Y., Drzewiecki, P.A., Moragas, M., Bover-Arnal, T., Macchiavelli, C., Wright, W., Messager, G., Embry, J.-C., Hunt, D., 2020. Tectono-sedimentary evolution of jurassic–cretaceous diapiric structures: Miravete anticline, Maestrat Basin, Spain. Basin Res. https://doi.org/10.1111/bre.12447.

Yose, L.A., Ruf, A.S., Strohmenger, C.J., Schuelke, J.S., Gombos, A., Al-Hosani, I., Al-Maskary, S., Bloch, G., Al-Mehairi, Y., Johnson, I.G., 2006. Three-dimensional characterization of a heterogeneous carbonate reservoir, lower cretaceous, abu dhabi (United Arab Emirates). In: Harris, P.M., Weber, L.J. (Eds.), Giant Hydrocarbon Reservoirs of the World: from Rocks to Reservoir Characterization and Modeling. AAPG Memoir 88/SEPM. Special Publication, pp. 173–212.

Yose, L.A., Strohmenger, C.J., Al-Hosani, I., Bloch, G., Al-Mehairi, Y., 2010. Sequence-stratigraphic evolution of an aptian carbonate platform (Shu'aiba Formation), eastern Arabian Plate, onshore abu dhabi, United Arab Emirates. In: van Buchem, F. S.P., Al-Husseini, M.I., Maurer, F., Droste, H.J. (Eds.), Barremian – Aptian Stratigraphy and Hydrocarbon Habitat of the Eastern Arabian Plate, vol. 2. GeoArabia Special Publication 4, Gulf PetroLink, Bahrain, pp. 309–340.